

H α Imaging of Early-type (Sa-Sab) Spiral Galaxies II: Global Properties ¹

Salman Hameed²

Five College Astronomy Department, Smith College, Northampton, MA 01063

shameed@ast.smith.edu

Nick Devereux

Department of Physics, Embry-Riddle Aeronautical University, Prescott, AZ 86301

devereux@erau.edu

ABSTRACT

New results, based on one of the most comprehensive H α imaging surveys of nearby Sa-Sab spirals completed to date, reveals early-type spirals to be a diverse group of galaxies that span a wide range in massive star formation rates. While the majority of Sa-Sab galaxies in our sample are forming stars at a modest rate, a significant fraction ($\sim 29\%$) exhibit star formation rates greater than $1 M_{\odot} yr^{-1}$, rivaling the most prolifically star forming late-type spirals. A similar diversity is apparent in the star formation history of Sa-Sab spirals as measured by their H α equivalent widths. Consistent with our preliminary results presented in the first paper in this series, we find giant H II regions ($L(H\alpha) \geq 10^{39} ergs^{-1}$) in the disks of $\sim 37\%$ of early-type spirals. We suspect that recent minor mergers or past interactions are responsible for the elevated levels of H α emission and perhaps, for the presence of giant H II regions in these galaxies. Our results, however, are not in total agreement with the H α study of Kennicutt & Kent who did not find any early-type spirals with H α equivalent widths $> 14\text{\AA}$. A close examination of the morphological classification of galaxies, however, suggests that systematic differences between the Revised Shapley Ames catalog and the Second Reference Catalog may be responsible for the contrasting results.

²Visiting Astronomer, Kitt Peak National Observatory (KPNO). KPNO is operated by the Association of Universities for Research in Astronomy, Inc. (AURA) under cooperative agreement with the National Science Foundation.

Subject headings: galaxies: evolution — galaxies: ISM — galaxies: photometry — galaxies: spiral — ISM: HII regions

1. Introduction

The last few decades have seen enormous progress in the understanding of star formation in spiral galaxies. While there is good agreement concerning the wide range of star formation rates seen among late-type spirals, different studies have yielded conflicting results for early-type (Sa-Sab) spiral galaxies. The H α equivalent width measurements of Kennicutt & Kent (1983) have been the most influential in establishing a dependence of massive star formation rates on spiral Hubble type, with early-type spirals emerging as galaxies with preponderantly low star formation rates, especially when compared to their later-type counterparts.

Other H α studies, however, find evidence for copious star formation in a significant fraction of the early-type spiral population. Young *et al.* (1996), Usui (1998) and Hameed & Devereux (1999) have identified numerous field early-type spirals with massive star formation rates comparable to Sc galaxies. The presence of such prolifically star forming early-type spirals weakens or completely removes the dependence of star formation rates along the spiral Hubble sequence.

The disparity of results regarding star formation rates in early-types spirals extends to other star formation indicators. For example, analyses of the far-infrared measurements (Devereux & Young 1990; Tomita, Tomita & Saito 1996; Devereux & Hameed 1997) were unable to reveal any dependence of massive star formation rates on spiral Hubble type. On the contrary, they were able to identify specific Sa-Sab galaxies with prodigious massive star formation as measured by their far-infrared emission. In contrast, Rieke & Lebofsky (1986) and Pompea & Rieke (1989) also analyzed the far-infrared data and found star formation rates to be inhibited in early-type spirals.

We have launched a systematic H α survey of early-type spirals in the local universe to quantify and analyze the properties of ionized gas in these galaxies in an effort to reconcile the conflicting results from earlier studies. Preliminary results, based on 27 galaxies, were

¹Based on observations obtained with the 3.5-meter telescope at Apache Point Observatory (APO) and the 0.9-meter telescope at Kitt Peak National Observatory (KPNO). The APO 3.5m telescope is owned and operated by the Astrophysical Research Consortium.

presented in Hameed & Devereux (1999; hereafter HD99). Here, we present the results of the entire sample. The sample is defined in §2 and the observations are described in §3. Our results are presented in §4, followed by a discussion in §5. Our conclusions are stated in §6.

2. The Sample

The galaxies have been selected from the Nearby Galaxy Catalog (NBG) (Tully 1988), which includes, among other galaxies, a list of all (74) *known* early-type spirals that are brighter than 12.0 magnitude and located within 40 Mpc. Our survey is motivated by the Infrared Astronomical Satellite (IRAS) survey that covered roughly 96% of the sky. The original goal of our survey was to image the 57, noninteracting, early-type (Sa-Sab) spirals that were also scanned by IRAS, that are brighter than $m(B)=12.1$, and have velocities less than 3000 km s^{-1} , placing them nearer than 40 Mpc ($H_0 = 75 \text{ km s}^{-1} \text{ Mpc}^{-1}$). All of these early-type spirals, with the exception of NGC 7727, were detected by the IRAS satellite.

$\text{H}\alpha$ images for 27 galaxies were presented in HD99, six of which have $m(B) > 12.1$ but were included because of their unusually high far-infrared luminosities (see HD99 for details). We have observed 18 additional early-type spirals, and have obtained $\text{H}\alpha$ images for six more galaxies from other sources. Thus, *the results presented in this paper are based on a sample of 51 early-type spirals*, 45 out of 57 ($\sim 79\%$) of which have $m(B) \leq 12.1$. Table 1 lists some useful observables for the target galaxies. Because of the limited resolution of IRAS satellite, our study excluded other spirals with cataloged companions within $3'$ of each other, thus eliminating almost all early-type spirals that are strongly interacting. While we would have liked to include all early-type spirals, ours constitutes essentially a complete sample and the $\text{H}\alpha$ images of 51 spirals presented herein should provide a representative picture of Sa-Sab galaxies in the local universe.

3. Observations

3.1. New $\text{H}\alpha$ Observations

Fourteen early-type spirals were observed using the direct CCD Imager on the 0.9 m telescope located at Kitt Peak National Observatory (KPNO) in Arizona. The imager used a 2048×2048 Tektronics chip and has a pixel scale of $0''.68 \text{ pixel}^{-1}$ at $f/7.5$, yielding a field of view of $23'.2 \times 23'.2$. All fourteen galaxies were imaged using the 72\AA , narrow-band, $\text{H}\alpha + [\text{NII}]$ (hereafter $\text{H}\alpha$, unless otherwise noted) filter centered at 6586\AA . The off-band images were obtained using the narrow-band line-free filter centered at 6487\AA ($\Delta\lambda = 67\text{\AA}$). Three

exposures of 1200 s were obtained through each of the line and continuum filters. Details of the observations are summarized in Table 2.

Three galaxies were imaged using the Seaver Prototype Imaging camera (SPIcam) on the Astrophysical Research Consortium (ARC) 3.5 m telescope at Apache Point Observatory (APO) in New Mexico. SPIcam uses a 2048×2048 CCD, has a pixel scale of $0''.14 \text{ pixel}^{-1}$, and a $4'.8$ field of view. The pixels were binned 2×2 in the readout, resulting in a pixel scale of $0''.28 \text{ pixel}^{-1}$. A 70\AA H α filter, centered at 6610\AA , and a 120\AA line-free continuum filter, centered at 6450\AA , were used to obtain the line and continuum images, respectively. Three exposures of 300 s were obtained through each of the line and continuum filters (Table 2).

NGC 2985 was observed using the Double Imaging Spectrograph (DIS) with the 3.5 m telescope at APO. DIS has a pixel scale of $0''.61 \text{ pixel}^{-1}$ and a $4'.2$ field of view. Three 390 s exposures were obtained through each of the line (6610\AA , $\Delta\lambda = 70\text{\AA}$) and the continuum (6450\AA , $\Delta\lambda = 120\text{\AA}$) filters (Table 2).

Observations for all galaxies were obtained under photometric conditions. The H α images were flux-calibrated using the standard stars BD $+28^{\circ}4211$, PG 0934+554, Feige 34, and HZ 44 (Massey *et al.* 1988). The data was reduced in the same manner as explained in HD99.

3.2. H α Data from Other Sources

Twenty-one galaxies from HD99 were observed with the 1.5 m telescope located at Cerro Tololo Inter-American Observatory (CTIO) in Chile. H α images for six galaxies were obtained with the ARC 3.5 m telescope located at Apache Point Observatory. Details of these observations are given in HD99.

NGC 3031 (M 81) was imaged by Devereux, Jacoby & Ciardullo (1995) with the Case Western Burrell Schmidt telescope at Kitt Peak National Observatory. The H α + [NII] image was obtained with a narrow-band, 74\AA , filter centered at 6568\AA . A narrow-band, 72\AA , line-free filter centered at 6481\AA , was used to obtain the continuum image. Results and analysis of the M 81 data are presented in Devereux, Jacoby & Ciardullo (1995).

Images for five galaxies (NGC 3705, NGC 4192, NGC 4419, NGC 4450, and NGC 4984) were kindly provided by Rebecca Koopman. All of these galaxies, except NGC 4984, were imaged with the 0.9 m telescope at KPNO. The H α image of NGC 4984 was obtained with the 0.9 m telescope located at CTIO. All of Koopman's images were obtained with a narrow-

band H α filter and a broadband R filter was used for the continuum images. Details of these observations are presented in Koopman (1997).

3.3. Comparison with Previous Studies

There are several galaxies in our survey that have published H α fluxes. Figure 1 compares H α fluxes for 15 galaxies measured by us in the same aperture as those in the literature. Figure 1 includes fluxes for seven galaxies published previously in HD99. Overall, there is good agreement between the measurements. There are, however, two exceptions. Our H α flux for NGC 4736 is 196% below the value obtained by Young *et al.* (1996) and our H α measurement for NGC 3718 is 180% above the value quoted by Young *et al.* (1996). Kennicutt & Kent (1983) also measured the H α flux of NGC 4736 and their value is within 29% of our measured flux. We do not know the reason for the difference of our flux value from that of Young *et al.*. However, we should note that there are 4 other galaxies that are in common with Young *et al.*’s sample, and their fluxes are within 2%(NGC 3504), 5%(NGC 660), 23%(NGC 2146), and 67%(NGC 3623) of our values. Overall, the mean ratio of our flux measurements to the other studies is 1.19 ± 0.6 . However, the ratio drops down to 1.10 ± 0.4 if we exclude NGC 3718 and NGC 4736.

3.4. Uncertainties in H α Flux and Equivalent Width Measurements

3.4.1. [NII] Contamination

The H α fluxes and H α equivalent widths presented in this paper include contributions from the two satellite [NII] lines at 6548Å and 6584Å. Complete inclusion of these lines in our line filters allows the possibility to later correct for [NII] contamination, when more information is available. Previous work has indicated that the [NII]/H α ratio varies from one galaxy to the next and within individual galaxies (Kennicutt & Kent 1983; Kennicutt 1992). A constant factor can, in principle, be used to correct for [NII] contamination. However, galaxy to galaxy variations are large enough to compromise this procedure. Kennicutt (1992) examined [NII]/H α ratios for 90 nearby galaxies, and found a median value close to 0.53 (excluding Seyfert galaxies). However, the mean ratio for 6 non-interacting Sa-Sab galaxies in his sample was 1.24 with ratios ranging from 0.48 up-to as high as 2.4. Furthermore, within a particular galaxy, the diffuse ionized gas has a higher value of [NII]/H α than H II regions (Greenawalt 1998). The [NII]/H α ratio is especially high in the central regions of galaxies, where H α absorption is strongest and [NII] is in emission (Young *et al.* 1996). Thus

we would need precise information about [NII]/H α ratio both within and among galaxies to properly correct for [NII] contamination.

3.4.2. *Extinction*

The H α fluxes presented in this paper have not been corrected for Galactic or internal extinction. Thus, the H α fluxes and luminosities we measure provide lower limits to the intrinsic H α fluxes and luminosities, and consequently to massive star formation rates. Kennicutt & Kent (1983) estimated, on average, 1 magnitude of extinction in their H α fluxes. However, extinction is expected to be higher for galaxies with high inclinations and for galaxies with dusty starbursts. Detailed studies of the highly disturbed early-type spirals, NGC 2146 and NGC 660, estimate 9 and 13 magnitudes of extinction in the visible, respectively (Young, Kleinmann & Allen 1988). In such extreme cases, Balmer recombination lines in the infrared, like Paschen α and Brackett γ , will be more suitable for determining star formation rates.

3.4.3. *Continuum Subtraction*

The continuum image for each galaxy was scaled to the line plus continuum image by measuring the integrated fluxes of 10-15 foreground stars common to both images. This scale factor, however, often needs adjustments, since the foreground stars and the galaxy are sometimes different in color. Adjustments were made iteratively until a satisfactory subtraction was obtained for the majority of the galaxy. The application of a constant scale factor across the entire galaxy introduces significant uncertainty, especially if there are large variations in color caused by changes in stellar populations. Often, the central regions are over-subtracted when the disk is well fit.

The uncertainty in the H α flux depends sensitively and non-linearly on the continuum level subtracted. This uncertainty is further aggravated by the contribution of the large stellar bulge in early-type spirals. For most galaxies in our sample, a 2-5% variation in the continuum level results in 10-50% errors in the H α flux, depending on the relative contribution of the continuum light. Flux measurements for NGC 4594 (The Sombrero galaxy) are particularly uncertain. This is an edge-on galaxy where the continuum light is completely dominated by the bulge. In the absence of a good view of the disk, it is very difficult to ascertain the true continuum level. A 3% variation in the continuum level of NGC 4594 results in a \sim 130% change in the measured H α flux.

3.4.4. Measurement of $H\alpha$ equivalent widths

$H\alpha$ equivalent widths are usually measured spectroscopically, however, images may also be used. The $H\alpha$ equivalent widths presented in this paper were calculated by dividing the continuum-subtracted $H\alpha$ emission line fluxes by the associated continuum flux and expressing the result in Angstroms (\AA) after the appropriate unit conversions. Unlike integrated spectroscopy, images provide additional information about the distribution of $H\alpha$ emission within a galaxy. For example, almost the entire $H\alpha$ emission of NGC 4369 is concentrated in the nuclear region. When measuring the continuum flux, we have included the full extent of the galaxy, which results in an $H\alpha$ equivalent width of 16.5\AA . However, if we use the continuum flux covering the same region as the $H\alpha$ emission, the value of $H\alpha$ equivalent width rises to 20.5\AA . In order to be consistent with existing spectroscopic measurements, we have used global $H\alpha$ and continuum fluxes for the determination of $H\alpha$ equivalent widths in this paper. However, we note in passing that this problem does not exist for late-type spirals where the massive star formation is usually spread throughout the entire disk and, as a result, is coextensive with the past star formation.

4. Results

4.1. Category 1 and Category 2 Early-type Spirals

The $H\alpha$ fluxes for 51 early-type spirals are presented in Table 3, along with the calculated $H\alpha$ luminosities and $H\alpha$ equivalent widths. In order to understand the diverse nature of early-type spirals, we have followed the division of Sa-Sab galaxies by HD99, based on the luminosity of the largest H II region in the disk of the galaxy. The motivation for this division comes from the studies of Kennicutt, Edgar, & Hodge (1989) and Caldwell *et al.* (1991), which did not find any H II regions with $H\alpha$ luminosity $\geq 10^{39} \text{ ergs}^{-1}$ in their samples of Sab and Sa galaxies, respectively. Thus, in our study, all H II regions in the disk of Category 1 early-type spirals have $L(H\alpha) < 10^{39} \text{ ergs}^{-1}$ whereas, Category 2 galaxies host at least one H II region *in the disk* with $H\alpha$ luminosity $\geq 10^{39} \text{ ergs}^{-1}$. We have also identified galaxies with intense nuclear starbursts (NGC 1022, NGC 1482, NGC 3885, NGC 3471) and have included them as Category 1 galaxies because they have virtually no disk $H\alpha$ emission. $H\alpha$ images for Category 1 and Category 2 galaxies are presented in Figures 2 and 3, respectively.

Figures 4 and 5 show the range of global $H\alpha$ luminosities and $H\alpha$ equivalent widths for the two categories of early-type spirals. As expected, Category 1 galaxies have preferentially lower global $H\alpha$ luminosities and smaller $H\alpha$ equivalent widths compared to Category 2 galaxies. The luminosity of the prototypical early-type spiral, M 81, is also marked on these

figures. Despite some overlap, a two-tailed Kolmogorov-Smirnov (K-S) test indicates that the two categories are not derived from the same population at a confidence level greater than 99%.

Within the current sample of 51 nearby galaxies, we find that 59% belong to Category 1. However, a significant fraction (37%) of early-type spirals, host giant H II regions in their disks. Two galaxies, NGC 660 and NGC 2146, have highly disturbed morphologies and have not been classified into either of the categories (HD99).

Despite having similar optical morphologies, early-type spirals show a wide diversity in H α morphology. Most Category 1 galaxies appear undisturbed in the continuum image, but exhibit diversity when it comes to the nuclear H α emission. Almost half (14/30) of all Category 1 galaxies host Extended Nuclear Emission-line Regions (ENER); a region of diffuse ionized gas in the nuclear region. As has been noted by Keel (1983), ENERs are only visible when there is very little or no star formation near the nucleus. In seven other Category 1 galaxies, it's hard to detect ENERs due to their high inclination. Two Category 2 galaxies (NGC 3169 and NGC 7213) also exhibit this diffuse gas. Seyfert nuclei have been identified in four Category 1 early-type spirals.

In HD99 we had speculated on a possible direct correspondence between the spectroscopic classification of LINERS and the morphologically identified ENERs. However, due to the small number of galaxies with spectroscopic classifications, we could not address that assertion statistically in that paper. Now, with a sample of 51 galaxies, we find that 12 Category 1 galaxies have been classified as LINERS, and 10 of those galaxies also show ENER emission, *suggesting an almost one-to-one correspondence between the spectroscopic and morphological classifications.*

The nuclei of Category 2 galaxies have been mostly classified as 'H' spectroscopically, indicating the presence of H II regions (Table 4). There are, however, four Category 2 galaxies with Seyfert nuclei. *The presence of equal numbers of Seyfert nuclei in each of the categories suggests that Seyfert activity is unrelated to the global star forming properties of early-type spiral galaxies.*

While the division of early-type spirals into two categories has been useful, we have to be cautious. First, it is difficult to measure the H α flux of an individual H II region. In HD99, we measured H α fluxes for the largest H II regions manually, using circular apertures. However, since then we have been using an automated program, "HIIphot" (See Thilker, Braun & Walterbos (2000) for details of the program), to determine the luminosity functions for star forming regions in spiral galaxies (Hameed, Thilker, & Devereux *in preparation*). All of our manual classifications are consistent with HIIphot, with the exception of NGC 3169 and

NGC 7213. Both of these galaxies host H II regions with $L(H\alpha) > 10^{39} \text{ ergs}^{-1}$, and thus have been classified as Category 2 galaxies in the current paper.

Second, we do not yet know of any physical significance of our classification scheme. A few studies, however, have suggested that the physical properties of H II regions change between $10^{38} - 10^{39} \text{ ergs}^{-1}$, such as the transition from normal “giant” H II regions to “supergiant” H II regions (Kennicutt, Edgar, & Hodge 1989), the transition from sparse embedded star clusters to dense embedded clusters in individual H II regions (Oey & Clark 1998), and the claim of the change from radiation bounded to density bounded H II regions (Beckman *et al.* 2000). Whatever the underlying significance of our scheme, it is of sufficient importance to report the detection of a significant fraction of early type spirals with giant H II regions, which is in contrast to the earlier findings of Kennicutt, Edgar, & Hodge (1989) and Caldwell *et al.* (1991).

4.2. $H\alpha$ vs. Far-infrared

The presence of massive stars can be traced via both $H\alpha$ and far-infrared emission. The relationship between the global $H\alpha$ and far-infrared (40-120 μm) luminosities is presented in Figure 6 for 51 Sa-Sab galaxies. Open dots represent Category 1 early-type spirals, Category 2 galaxies are represented by solid dots, and the two unclassified galaxies, NGC 660 and NGC 2146, have been plotted as stars. The far-infrared luminosity, $L(\text{FIR})$, has been calculated using,

$$L(40 - 120\mu\text{m}) = 3.65 \times 10^5 S(\text{FIR}) D^2 L_\odot$$

where $S(\text{FIR}) = (2.58 S_{60\mu\text{m}} + S_{100\mu\text{m}})$ and D is the distance expressed in Mpc. The values $S_{60\mu\text{m}}$ and $S_{100\mu\text{m}}$ are fluxes measured by the Infrared Astronomical Satellite (IRAS) in units of Jy. The solid lines in Figure 6 identify ratios of $L(\text{FIR})/L(H\alpha)$ expected for H II regions, ionized by massive stars ranging in spectral type from O5 to B5. The ratios are based on a simple model of an idealized H II region, in which all photons shortward of the Lyman limit are absorbed by the hydrogen gas while the bolometric luminosity of the star is absorbed by surrounding dust and re-radiated in the far-infrared (Panagia 1973; Devereux & Young 1990).

Figure 6 shows that most early-type spirals in our sample, including M 81 (NGC 3031), have $L(\text{FIR})/L(H\alpha)$ ratios consistent with those expected for H II regions. However, there are some galaxies that have unusual ratios. Most of the errant galaxies either host a Seyfert nucleus (NGC 4151, NGC 2273, NGC 7172) or are nuclear starbursts (NGC 1022, NGC 1482). Non-stellar emission from Seyfert galaxies is not expected to follow the $L(\text{FIR})/L(H\alpha)$ ratios for massive stars, whereas, the unusual location of nuclear starburst galaxies in Figure

6 may be due to high dust extinction. Similarly, the locations of NGC 660 and NGC 2146 may be explained by the 13 and 9 magnitudes of extinction, respectively (Young, Kleinmann & Allen 1988). The nucleus of NGC 5188 is spectroscopically classified as “H” by Veron-Cetty & Veron (1986). However, we detect an unresolved H α nuclear point source (HD1999) and suspect that its has a Seyfert nucleus that may have been missed in the earlier spectroscopic study. The remaining 4 outlying galaxies (NGC 1371, NGC 3718, NGC 4419, NGC 4845) warrant additional scrutiny to fully understand the reason for their unusual ratios.

Another word of caution here. Despite the fact that massive stars appear to be capable of sustaining the H α and far-infrared luminosities in most galaxies, detailed studies of the nearest spiral galaxies have indicated that a sizable fraction of the bulge far-infrared and H α emission is not powered by massive stars at all (Devereux *et al.* 1994; Devereux, Jacoby & Ciardullo 1995). Approximately 30% of the total far-infrared and H α emission from M 31 and M 81 originates from the bulge. This bulge H α emission is diffuse in nature, much like the ENERs, and observations with the Hubble Space Telescope have convincingly shown the absence of massive stars in the central regions of these two galaxies (Devereux, Ford & Jacoby 1997). As mentioned in § 4.1, almost half of all Category 1 early-type spirals host this diffuse H α emission in the nuclear region. The source of the H α emission is unknown, however, it is unlikely to be ionized by a central AGN in all cases, as the luminosity of the extended region far exceeds that of the nucleus itself in several galaxies. On the other hand an extended region of ionization could be sustained by bulge post-asymptotic giant branch (PAGB) stars or by collision induced shocks occurring within the bulge gas itself (Heckman 1996). The same bulge PAGB stars may also be responsible for heating the dust that gives rise to the diffuse bulge far-infrared emission.

Figure 7 investigates the correlation between L(FIR)/L(B) and H α equivalent widths for all 51 galaxies in our sample. Both quantities measure the ratio of present to past star formation, where the present star formation rate is determined by far-infrared and H α emissions and are normalized by past star formation as traced by blue and red continuum luminosities, respectively. Figure 7 shows that, overall, there is a trend between H α equivalent width and L(FIR)/L(B), but it is not a one-to-one correlation. In general, galaxies with low L(FIR)/L(B) have low H α equivalent widths, and galaxies with high values of L(FIR)/L(B) have high H α equivalent widths. A Spearman’s Rank Correlation test gives a value of 0.68, suggesting a weak correlation. The least-square fitting to the data gives a slope of 0.47. Note that some of the galaxies with excess L(FIR)/L(B) are also the outliers in Figure 6 and vice versa. Heavy extinction may be responsible for the shallow slope of the relation. Usui (1998), based on a study of 15 galaxies, find a slope of 0.82 for L(FIR)/L(B) versus H α equivalent widths for early-type spirals with high EW(H α) > 3 \AA , and a correlation coefficient of 0.79. Our results do not change significantly even after restricting our sample

to galaxies with $\text{EW}(\text{H}\alpha) > 3\text{\AA}$.

4.3. $\text{H}\alpha$ Equivalent width vs. (B-V)

The relationship between the $\text{H}\alpha$ equivalent widths and $(\text{B-V})_e$ colors for 49 early-type spirals is illustrated in Figure 8. $(\text{B-V})_e$ colors are adopted from the Third Revised Catalog of Bright Galaxies (de Vaucouleurs *et al.* 1991). NGC 4750 and UGC 3580 do not have $(\text{B-V})_e$ measurements, and hence are not included here. Figure 8 shows that early-type spirals exhibit a wide range of $\text{H}\alpha$ equivalent widths and $(\text{B-V})_e$ colors, much wider than previously reported for early-type spirals by Kennicutt (1983). Furthermore, the $\text{H}\alpha$ equivalent widths and $(\text{B-V})_e$ colors are correlated. A non-parametric Spearman rank correlation test allows the null hypothesis, that the two observables are not correlated, to be rejected at $> 99.9\%$ significance level.

As noted by Kennicutt (1983), the relationship between the $\text{H}\alpha$ equivalent widths and (B-V) colors can, in principle, provide useful constraints on the past star formation history. By way of illustration, the range of plausible star formation histories permitted by the new observations is also indicated in Figure 8. The solid lines in Figure 8 illustrate the loci of model $\text{H}\alpha$ equivalent widths and $(\text{B-V})_e$ colors expected for a 15 billion year old galaxy that has evolved at different rates. There are two curves plotted, each running from upper left to lower right. The left curve represents zero extinction, the right curve includes the extinction expected for a galaxy viewed essentially edge-on ($i = 85^\circ$). The flatter dashed lines joining points on the two curves show the direction of reddening vectors. The results are based on a spectrophotometric evolution model for starbursts and galaxies called PEGASE (Fioc & Rocca-Volmerange 1997; Moy, Rocca-Volmerange, & Fioc 2001).

The details of the PEGASE evolutionary models are presented in Fioc & Rocca-Volmerange (1997); Moy, Rocca-Volmerange, & Fioc (2001). Briefly, the model evolves stars with a range of stellar metallicities from the main sequence, to the He flash, the horizontal branch, the asymptotic giant branch, and finally to demise as supernova or white dwarfs. The star formation scenarios used here are similar to those adopted by Kennicutt (1983); an exponential star formation law with an “extended” Miller-Scalo initial mass function, and stellar masses ranging from $0.1 - 100 \text{ M}_\odot$. PEGASE calculates broad band colors as well as nebular emission. Additionally, radiative transfer computations provide an internally consistent estimate of dust extinction in the model galaxy.

The blue color and high $\text{H}\alpha$ equivalent width combination at the upper left of Figure 8 denotes a galaxy that has been converting gas into stars at essentially a constant rate

since birth. The reddest colors and smallest $\text{H}\alpha$ equivalent widths at the lower right of the diagram denotes a star formation history in which most of the primordial gas was rapidly converted into stars some 3×10^{10} years after galaxy formation. Most early-type spirals lie between the two extremes described above. Thus, the PEGASE results indicate that the star formation history of early-type spirals is diverse; a further testament to their heterogeneous nature already apparent from the $\text{H}\alpha$ images. It is quite remarkable indeed that a history of continuous star formation, or a continuously decreasing star formation rate, together with the effects of reddening, can explain the wide range of colors and $\text{H}\alpha$ equivalent widths observed for the majority of early-type spirals plotted in Figure 8.

Interestingly, the correlation between the $\text{H}\alpha$ equivalent widths and $(\text{B}-\text{V})_e$ colors breaks down for the objects with the highest $\text{H}\alpha$ equivalent widths (i.e. $> 14\text{\AA}$), a result that is substantiated by a Spearman rank correlation test. Part of the reason may be attributed to the presence of active galactic nuclei (AGNs). NGC 4151, for example, is a well-known Seyfert 1 galaxy, and NGC 2273 and NGC 6810 are Seyfert 2's (Ho, Filippenko, & Sargent 1997; Veron-Cetty & Veron 1986). However, not all AGNs exhibit unusual colors in Figure 8. Conversely, not all of the errant points in Figure 8 can be attributed to AGNs. NGC 1482 and NGC 972, for example, have no documented evidence for an AGN and yet they are among the most deviant of all the outliers in Figure 8. The $\text{H}\alpha$ images show evidence for a nuclear starburst in NGC 1482, and extended nuclear star formation activity in NGC 972. The unusually high $\text{H}\alpha$ equivalent widths, given the red colors of NGC 1482 and NGC 972, are in fact, exactly what one would expect for a recent starburst superimposed on an older population. The high $\text{H}\alpha$ equivalent widths indicate that the starburst increased the star formation activity by at least one order of magnitude over the pre-existing rate. Interestingly, recent HI observations of NGC 972 reveal a tidal tail in neutral hydrogen indicative of a past interaction (Hameed & Young 2003). Note, however, that *not all* interacting early-type spirals have unusual colors. For example, M81 (Yun, Ho, & Lo 1994), NGC 3471 (Hameed & Young 2003), NGC 3885 (Hameed & Young 2003), NGC 4725 (Wevers *et al.* 1984) show interaction signatures in HI and yet have colors and $\text{H}\alpha$ equivalent widths that can be explained by a "normal" star formation history.

We caution that PEGASE interprets global measurements, which do not constrain or preclude different star formation histories *within* individual galaxies. Nevertheless, the star formation histories of early-type spirals as revealed by their global $(\text{B}-\text{V})_e$ colors and $\text{H}\alpha$ equivalent widths are considerably more diverse than had previously been appreciated (e.g. Kennicutt (1983)). We have also included Kennicutt's Sa-Sab galaxies in Figure 8, most of which have preferentially smaller $\text{H}\alpha$ equivalent widths and redder colors. We will explore some of the reasons for these differences in § 5.

4.4. Massive Star Formation Rates

The ionizing flux from galaxies can be converted to star formation rates using evolutionary synthesis models and by making assumptions regarding abundances and the shape of the initial mass function (IMF) (Kennicutt, Tamblyn & Congdon 1994; Kennicutt 1998). While we can, under some circumstances, measure low mass star formation in nearby molecular clouds in our own Galaxy, such measurements are impossible for external galaxies. Nevertheless, we have calculated total (low mass plus high mass) star formation rates using Kennicutt's (1998) conversion:

$$SFR(M_{\odot}yr^{-1}) = 7.9 \times 10^{-42} L(H\alpha)(ergs\ s^{-1})$$

assuming solar abundances, a Salpeter IMF (0.1-100 M_{\odot}), and a Case B recombination at $T_e=10,000$ K. We find that the average star formation rate for our entire sample is $0.94\ M_{\odot}yr^{-1}$ with 29% of early-type spirals having star formation rates in excess of $1\ M_{\odot}yr^{-1}$, up to a maximum of $3.5\ M_{\odot}yr^{-1}$.

While these calculations are interesting, they should be regarded with caution. Apart from the usual concerns regarding the shape and extent of the IMF, there are observational uncertainties that can affect the measured star formation rates. For example, we have not corrected our $H\alpha$ fluxes for extinction (see § 3.4.2) and yet numerous galaxies in our sample harbor starbursts in their nuclear regions or exhibit prominent dust lanes. The extinction in the optical can be as high as 13 magnitudes as seen in NGC 2146 (Young, Kleinmann & Allen 1988). Thus the calculated star formation rates certainly represent a lower limit, and in some cases they may be underestimated by an order of magnitude. Second, the conversion factor used to calculate star formation rates assumes that almost all of the $H\alpha$ emission is coming from H II regions, but we have discovered that ENER's are common in early-type spirals, consequently not all the $H\alpha$ emission can be attributed to massive star formation. While the above mentioned problems may be important in individual cases, these do not affect our overall conclusions regarding star formation rates in early-type spirals as none of these special circumstances ever dominate the global $H\alpha$ emission of the galaxies, except in the case of NGC 4151, where the majority of the $H\alpha$ emission is coming from the Seyfert nucleus.

5. Discussion

5.1. The Ratio of Present to Past Star Formation Rates

Our comprehensive volume limited H α survey has exposed the heterogeneous nature of nearby early-type spirals. Perhaps the most surprising result, first suggested in HD99, is the discovery that a significant fraction of Sa-Sab galaxies host giant H II regions and levels of H α emission comparable to those seen in nearby late-type spirals.

The popular perception that early-type spirals are currently associated with low levels of star formation is primarily due to the H α equivalent width results of Kennicutt & Kent (1983). The star formation history of galaxies can be traced using H α equivalent widths, where the current star formation, as measured by the H α emission, is normalized by the red continuum light which represents the past star formation integrated over the lifetime of the galaxy. Figure 9 compares H α equivalent widths of 51 Sa-Sab galaxies in our sample with those of Kennicutt & Kent. The top panel shows that early-type spirals exhibit a wide range of H α equivalent widths, much wider than the Sa-Sab galaxies in the Kennicutt & Kent (1983) sample which have preferentially low H α equivalent widths (second panel in Figure 9). Over half of Kennicutt & Kent's measurements are upper limits. Of the remaining detections, none exceed H α equivalent widths of 14Å. In comparison, about 35% of early-type spirals in our sample have H α equivalent widths $> 14\text{\AA}$.

The third panel of Figure 9 shows H α equivalent widths for early-type spirals included in Usui (1998). However, their study focused only on those Sa-Sab galaxies that have high L(FIR)/L(B) ratios. Consequently, one can expect the H α equivalent widths in their sample to have preferentially higher values because of the correlation in Figure 7 described previously in section 4.2. Combining L(FIR)/L(B) luminosity ratios (Tomita, Tomita & Saito 1996) and H α equivalent widths, Usui *et al.* estimated that 30% of early-type spirals must have H α equivalent widths greater than 20Å. We confirm their prediction, since we find 28% of Sa-Sab galaxies in our sample with H α equivalent widths $> 20\text{\AA}$. Figure 9 also includes H α equivalent widths for 20 Sa-Sab galaxies taken from a recent survey of 334 galaxies across all Hubble types, conducted by James *et al.* (2004). While missing the very high star forming early-type spirals, the James *et al.* (2004) sample still display a range of H α equivalent widths that is broader than Kennicutt & Kent (1983). *Overall, our survey of early-type spirals encompasses the range of H α equivalent widths observed by Kennicutt & Kent (1983), Usui (1998), and James *et al.* (2004).*

Seyfert galaxies were not included in the Kennicutt & Kent (1983) and Usui (1998) samples. The non-stellar emission from Seyfert nuclei can potentially increase the H α equivalent widths of galaxies, although it is really obvious only for one galaxy in our sample;

NGC 4151. Nevertheless, in order to remove any doubt over the influence of Seyferts, we have plotted our H α equivalent widths again in the bottom panel of figure 9 after excluding the nine Seyferts in our sample. The overall trend of H α equivalent widths is unaffected, suggesting that the presence of Seyfert nuclei does not dominate the global H α emission of these early-type spiral galaxies.

5.2. Morphological Classifications: RC2 vs RSA

There are at least two reasons for the differences between our results and those of Kennicutt & Kent (1983). First, a significant fraction of the early-type spirals with high H α equivalent widths reside in the southern hemisphere, and most galaxies in Kennicutt & Kent’s sample are located in the northern hemisphere. The biggest factor, however, may be the systematic difference in the morphological classification of galaxies between the Revised Shapley Ames Catalog (RSA; Sandage & Tammann (1981)) used by Kennicutt & Kent (1983) and the Nearby Galaxy Catalog (NBG; Tully (1988)) used by us. The NBG adopted most of the morphological classifications from the Second Reference Catalog (RC2; de Vaucouleurs, de Vaucouleurs, & Corwin (1976)). We have listed the classifications from all three catalogs in Table 5 for the early-type spirals in our study. There is, in general, good agreement among the different catalogs for Category 1 early-type spirals. For Category 2 galaxies, however, the RSA has systematically classified them as later-type galaxies. Figure 10 illustrates systematic differences in classification between the RSA and RC2. Whereas, the misclassifications in Category 1 galaxies tend to be random, the misclassifications of Category 2 galaxies are biased toward the later types.

HD99 related the reason for these systematic differences to the subtle differences in the criteria used to classify spiral galaxies. The RC2 catalog uses all three Hubble criteria for classifying spiral galaxies: the size of the bulge, the pitch angle, and the resolution of spiral arms (de Vaucouleurs 1959). On the other hand, RSA classifications of spiral galaxies are based only on the characteristics of spiral arms (Sandage 1961), which, in turn, are directly correlated with star formation. The Carnegie Atlas of Galaxies (Sandage & Bedke 1994) suffers from the same morphological bias: whereas the resolution of spiral arms in the Carnegie Atlas is replaced by a more useful parameter, the star formation rate, as determined by the H α emission, the classification of Sa-Sab galaxies still follows those of the RSA catalog. This is surprising since the Carnegie Atlas, unlike the RSA catalog, proclaims to include bulge size as one of the classification criterion. However, a closer inspection of the two catalogs shows that the classifications of Sa and Sab galaxies are almost identical with only one exception: NGC 5121 changed from being an S0(4)/Sa in the RSA to an Sa in the

Carnegie Atlas.

Thus, we maintain that the wide variety of results in the published literature concerning the systematics of massive star formation along the Hubble sequence can be traced directly to these subtle differences in classification schemes between the RSA and the RC2. Kennicutt & Kent (1983), quite likely overlooked several of the most prolifically star forming early-type spirals because they were classified as later type spirals in the RSA catalog. Our view today of massive star formation along the spiral Hubble sequence may have been quite different if previous investigators had exclusively adopted the RC2 classification scheme.

5.3. Interaction-induced Massive Star Formation?

One of the most important results from our survey has been the discovery of a significant fraction of early-type spirals with giant H II regions and star formation rates comparable to those found in late-type spirals. Since the majority of Sa-Sab galaxies have more modest star formation rates, it is pertinent to ask if those with high star formation rates are going through a temporary phase of enhanced star formation?

Studies over the past decade have exposed dynamical or morphological anomalies such as counter-rotating disks, shells, and disturbed bulges, in a number of early-type spirals. Such features represent the fossilized signatures of an interaction or a minor merger that occurred in the distant past (Schweizer 1990; Hernquist & Spergel 1992). While most of these galaxies are quiescent today, they may well have experienced a temporary phase of enhanced star formation during a gravitational encounter with another galaxy.

It is well established that interacting galaxies exhibit higher levels of H α (Kennicutt *et al.* 1987) and FIR emission (Bushouse 1987) compared to a sample of isolated galaxies, suggesting elevated levels of star formation. We suspect that a large fraction of nearby early-type spirals are going through an interaction or are in the process of swallowing a smaller galaxy. Tentative support for this idea comes from recent HI observations. In a study of 7 Sa-Sab galaxies with high levels of H α emission, Hameed & Young (2003) find unambiguous signs of recent interactions in 6 of these galaxies. Interaction signatures include HI tidal tails (NGC 972, NGC 3885, NGC 7213) and neutral hydrogen bridges connecting neighboring galaxies (NGC 3471, NGC 5915, NGC 7582).

Some of the dispersion seen in the H α equivalent width vs (B-V) plot of Figure 8 may also be attributed to interactions. Kennicutt *et al.* (1987) find a similar dispersion in their sample of interacting galaxies that can be explained by superimposing a burst of star formation on an evolved stellar population. The strength of the burst and the location of a

galaxy on the plot, of course, depends on a number of parameters including the extinction, the gas content, and the orbital parameters of the interaction. Nevertheless, the dispersion of colors and H α equivalent widths seen among early-type spirals is reminiscent of that seen among the interacting galaxies, providing further support for the idea that elevated star formation may only be a temporary phase for these nearby early-type spirals.

It should be noted, however, that not all interacting early-type spirals exhibit unusually high FIR or H α emissions. For example, HI maps of M81 (Yun, Ho, & Lo 1994), NGC 3368 (Schneider 1989), and NGC 4725 (Wevers *et al.* 1984) reveal unambiguous interaction signatures and yet H α imaging reveals relatively little evidence for enhanced star formation. On the other hand, it is to be expected that the HI signature of an interaction will last far longer than the associated episode of massive star formation that the interaction causes.

5.4. Influence of Bars on Early-type Spirals

It is now well documented that the presence of a bar in a galaxy can induce star formation either at the ends of the bar or in the nuclear and circum-nuclear regions. The influence of bars on global star formation rates has been the subject of many studies over the past few decades and has led to the consensus that there are no significant differences in *global* massive star formation rates between barred and unbarred galaxies (e.g. Ryder & Dopita (1994); Tomita, Tomita & Saito (1996)). However, there is some evidence that nuclear star formation appears to be enhanced in early-type barred spirals compared to their unbarred counterparts (Devereux 1987; Huang *et al.* 1996; Ho, Filippenko, & Sargent 1997). Such an effect is not seen in late-type spiral galaxies and may be related to the location of the inner Lindblad resonance (ILR), which is dependent on the central mass distribution. The ILR in an early-type spiral is expected to be located inside the bar and closer to the nucleus than in a late-type spiral (Elmegreen & Elmegreen 1985) and thus can transfer gas more efficiently to the central region of the galaxy, triggering star formation. It should be noted, however, that not all barred early-type spirals have enhanced nuclear star formation; thus the mere presence of a bar is not sufficient for nuclear star formation to occur.

Our sample of 51 Sa-Sab galaxies provides an ideal opportunity to study the effects of bars on these bulge-dominated galaxies. Our sample includes 29 barred galaxies (including the intermediate types classified as 'X' in the Nearby Galaxies Catalog (Tully 1988) or 'SAB' in the RC2 catalog (de Vaucouleurs 1959)), 17 unbarred galaxies and 5 galaxies with no classification (Table 4). Figure 11 shows the histogram of the ratio of H α emission from the central 1 kpc (diameter) region to the total H α emission for barred and unbarred early-type spirals. We do not find a statistically significant difference between barred and unbarred

galaxies in the fraction of the global H α emission that is radiated by the nucleus. Similarly, figure 12 plots the total H α luminosity against the ratio of nuclear to total H α luminosity, and again we find no effect due to the presence of a bar. However, the histogram of nuclear (1-kpc) H α luminosity (Figure 13) appears to be slightly enhanced in barred early-type spirals compared to unbarred galaxies, consistent with earlier studies (Devereux 1987; Huang *et al.* 1996; Ho, Filippenko, & Sargent 1997).

Thus, we find some evidence that bars in early-type spirals may enhance the nuclear H α luminosity, but the picture is far from clear. We have examples of barred galaxies with nuclear starbursts (e.g. NGC 3504, NGC 1022), barred galaxies with virtually no star formation in the nuclear region (e.g. NGC 1398, NGC 1350), unbarred galaxies with nuclear starbursts (e.g. NGC 3885) and an unbarred galaxy, NGC 7213, with a circumnuclear star forming ring.

6. Conclusions

We have presented results from an H α imaging survey of 51 nearby Sa-Sab galaxies. Our images indicate that, contrary to popular perception, early-type spirals are, in fact, a diverse group of galaxies that span a wide range of massive star formation rates and star formation histories. Some of the diversity is attributed to ongoing star formation induced by interactions or mergers. Our H α images also show that giant H II regions ($L(H\alpha) \geq 10^{39} \text{ ergs}^{-1}$) do exist in the disks of some early-type spirals thereby dispensing with the need for a special, different, or biased initial mass function in early type spirals. Additionally, we have established an essentially one to one correspondence between the spectroscopically classified LINERS and the existence of an extended and diffuse component of H α emission under the bulges of the LINER host galaxies. We also find a systematic difference between the morphologies of galaxies in the Revised Shapley Ames Catalog and the Second Reference Catalog that may be responsible for the contrasting results in the published literature concerning massive star formation rates among the Hubble sequence of spiral galaxies.

The authors would like to thank Rene' Walterbos for providing the H α filter set for the APO observations and the staff at APO and KPNO for their expert assistance at the telescopes. We would also like to thank the referee for useful comments that improved the presentation of the paper.

REFERENCES

Ashby,M.L.N., Houck,J.R., & Matthews,K. 1995, ApJ, 447, 545

Beckman, J. E., Rozas, M., Zurita, A., Watson, R. A. & Knapen, J. H. 2000, AJ, 119, 2728

Balzano,V.A. 1983, ApJ, 268, 602

Bushouse,H.A. 1987, ApJ, 320, 49

Caldwell, N, Kennicutt, R. C., Jr, Phillips, A. C., & Schommer, R. A. 1991, ApJ, 370, 526

de Vaucouleurs, G. 1959, *Handbuch der Physik*, vol. 53, 275 (Berlin: Springer-Verlag)

de Vaucouleurs, G., de Vaucouleurs,A., & Corwin,H.G., Buta, R. J., Paturel, G. & Fouque, P. 1991, *Third Reference Catalogue of Bright Galaxies* (Springer-Verlag)

de Vaucouleurs, G., de Vaucouleurs,A., & Corwin,H.G. 1976, *Second Reference Catalog of Bright Galaxies* (University of Texas, Austin) (RC2)

Devereux, N. A. 1987, ApJ, 323, 91

Devereux, N. A., Ford, H. & Jacoby, G. 1997, ApJ, 481, L71

Devereux,N.A., & Hameed,S. 1997, AJ, 113, 599

Devereux,N.A., Jacoby,G., & Ciardullo,R. 1995, AJ, 110, 1115

Devereux, N. A., Price, R., Wells, L. A. & Duric, N. 1994, AJ, 108, 1667

Devereux, N. A., & Young, J. S. 1990, ApJ, 350, L25

Elmegreen, B. G. & Elmegreen, D. M. 1985, ApJ, 288, 438

Filippenko,A.V., & Halpern,J.P. 1984, ApJ, 285,458

Fioc, M. & Rocca-Volmerange, B. 1997, A&A, 326, 950

Freedman, W. L. *et al.* 2001, ApJ, 553, 47

Greenawalt, B. 1998, PhD. Thesis, New Mexico State University, Las Cruces, New Mexico

Hameed, S., & Devereux, N. A. 1999, AJ, 118, 730 (HD99)

Hameed, S. & Young, L. M. 2003, AJ, 125, 3005

Heckman, T. M. 1996, in *The Physics of LINERS in view of Recent Observations*, ed. Eracleous, M., Koratkar, A., Leitherer, C., & Ho, L. (ASP Conference Series Volume 103)

Hernquist, L. & Spergel, D. N. 1992, ApJ, 399, L117

Ho, L. C., Filippenko, A. V., & Sargent, W. L. W. 1997, ApJS, 112, 315

Huang, J. H., Gu, Q. S., Su, H. J., Hawarden, T. G., Liao, X. H. & Wu, G. X. 1996, 1996, A&A, 313, 13

James, P.A., Shane, N.S., Beckman, J.E., Cardwell, A., Collins, C.A., Etherton, R.S., de Jong, R.S., Fathi, K., Knapen, J.H., Peletier, R.F., Percival, S.M., Pollacco, D.L., Seigar, M.S., Stedman, S., and Steele, I.A 2004, A&A, 414, 23

Keel, W. B. 1983, ApJ, 268, 632

Kennicutt, R.C., Jr. 1998, *Ann. Rev. Astron. Astrophys.*, 36, 189

Kennicutt, R. C., Jr. 1992, ApJ, 388, 310

Kennicutt, R. C., Jr. 1983, ApJ, 272, 54

Kennicutt, R.C., Jr., Edgar, K.B., & Hodge, P.W., 1989, ApJ, 337, 761

Kennicutt, R.C., Jr., & Kent, S.M. 1983, AJ, 88, 1094

Kennicutt, R.C., Jr., Roettiger, K. A., Keel, W. C., van der Hulst, J. M., Hummel, E. 1987, AJ, 93, 1011

Kennicutt, R. C., Jr., Tamblyn, P, Congdon, C. E. 1994, ApJ, 435, 22

Koopman, R. PhD. Thesis, Yale University, New Haven, Connecticut

Lehnert, M.D., & Heckman, T.M. 1995, ApJS, 97, 89

Massey, P., Strobel, K., Barnes, J.V., & Anderson, E. 1988, ApJ, 328, 315

Moy, E., Rocca-Volmerange, B., & Fioc, M. 2001, A&A, 365, 347

Oey, M. S. & Clarke, C. J. 1998, AJ, 115, 1543

Panagia, N. 1973, AJ, 78, 929

Phillips, M.M., Charles, P.A., & Baldwin, J.A. 1983, ApJ, 266, 485

Pompea,S.M., & Rieke,G.H. 1989, ApJ, 342, 250

Rieke, G. H. & Lebofsky, M. J. 1986, ApJ, 304, 326

Ryder, S. D. & Dopita, M. A. 1994, ApJ, 430, 142

Sandage,A.R. 1961, *The Hubble Atlas of Galaxies*, Publ. No. 618 (Carnegie Institution of Washington, Washington,D.C.)

Sandage, A. & Bedke, J. 1994, *The Carnegie atlas of galaxies*, (Carnegie Institution of Washington with The Flintridge Foundation)

Sandage,A., & Tammann,G.A. 1981, *A Revised Shapley-Ames Catalog of Bright Galaxies*, Publ. No. 635 (Carnegie Institution of Washington, Washington,D.C.) (RSA)

Schneider, S. E. 1989, ApJ, 343, 94

Schweizer,F. 1990, in *Dynamics and Interactions of Galaxies*, ed. Wielen.R. (Heidelberg: Springer-Verlag)

Sharples,R.M., Longmore,A.J., Hawarden,T.G., and Carter,D. 1984, MNRAS, 208, 15

Thilker, D., Braun, R., Walterbos, R. A. M. 2000, AJ, 120, 3070

Tomita, A., Tomita, Y., and Saito, M. 1996, PASJ, 48, 285

Tully,R.B. 1988, *Nearby Galaxies Catalog* (Cambridge: Cambridge University Press)

Unger,S.W., Lawrence,A., Wilson,A.S., Elvis,M., and Wright,A.E. 1987, MNRAS, 228, 521

Usui, T., Saito, M., and Tomita, A. 1998, AJ, 116, 2166

Veron-Cetty, M. P., & Veron, P. 1986, A&AS, 66,335

Wevers, B. M. H. R., Appleton, P. N., Davies, R. D. & Hart, L. 1984, A&A, 140, 125

Young,J.S., Allen,L., Kenney,J.D.P., Lesser,A., & Rowand,B. 1996, AJ, 112, 1903

Young, J. S., Kleinmann, S. G. & Allen, L. E. 1988, ApJ, 334, L63

Yun, M. S., Ho, P. T. & Lo, K. Y. 1994, Nature, 372, 530

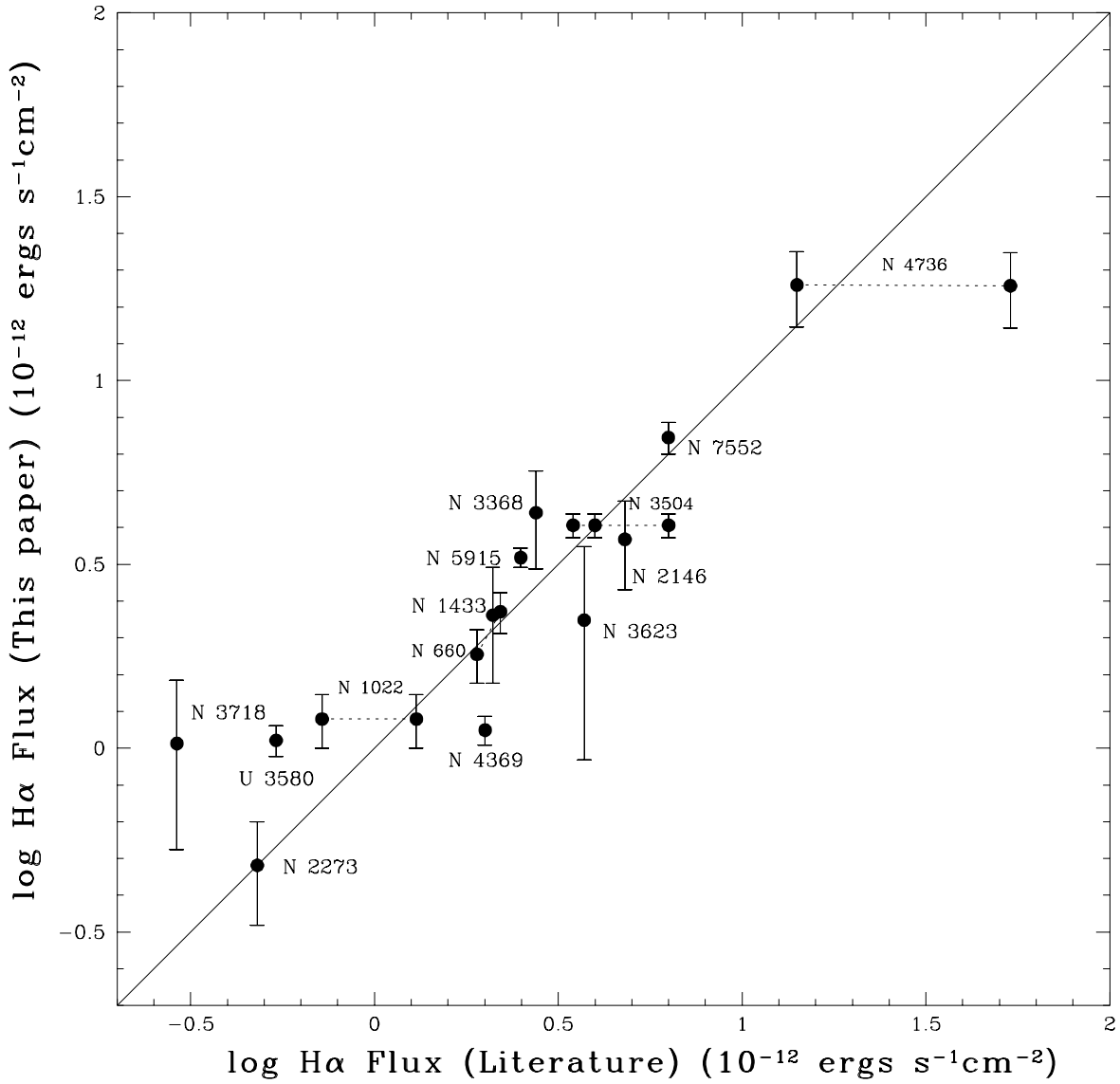


Fig. 1.— Comparison of H α measurements taken from the literature with those measured from our H α images using the same aperture size (when available). NGC 660, NGC 1022 and NGC 4736 have two comparison measurements, whereas, NGC 3504 has three published values.

Fig. 2.— a-d: Red continuum and continuum-subtracted $\text{H}\alpha$ images of 12 Category 1 early-type spiral galaxies. North is at the top and east is at the left in each image. The white bar in the bottom left-hand corner of each image represents 1 kpc in length.

Fig. 3.— a-b: Red continuum and continuum-subtracted H α images of 6 Category 2 early-type spiral galaxies. North is at the top and east is at the left in each image. The white bar in the bottom left-hand corner of each image represents 1 kpc in length.

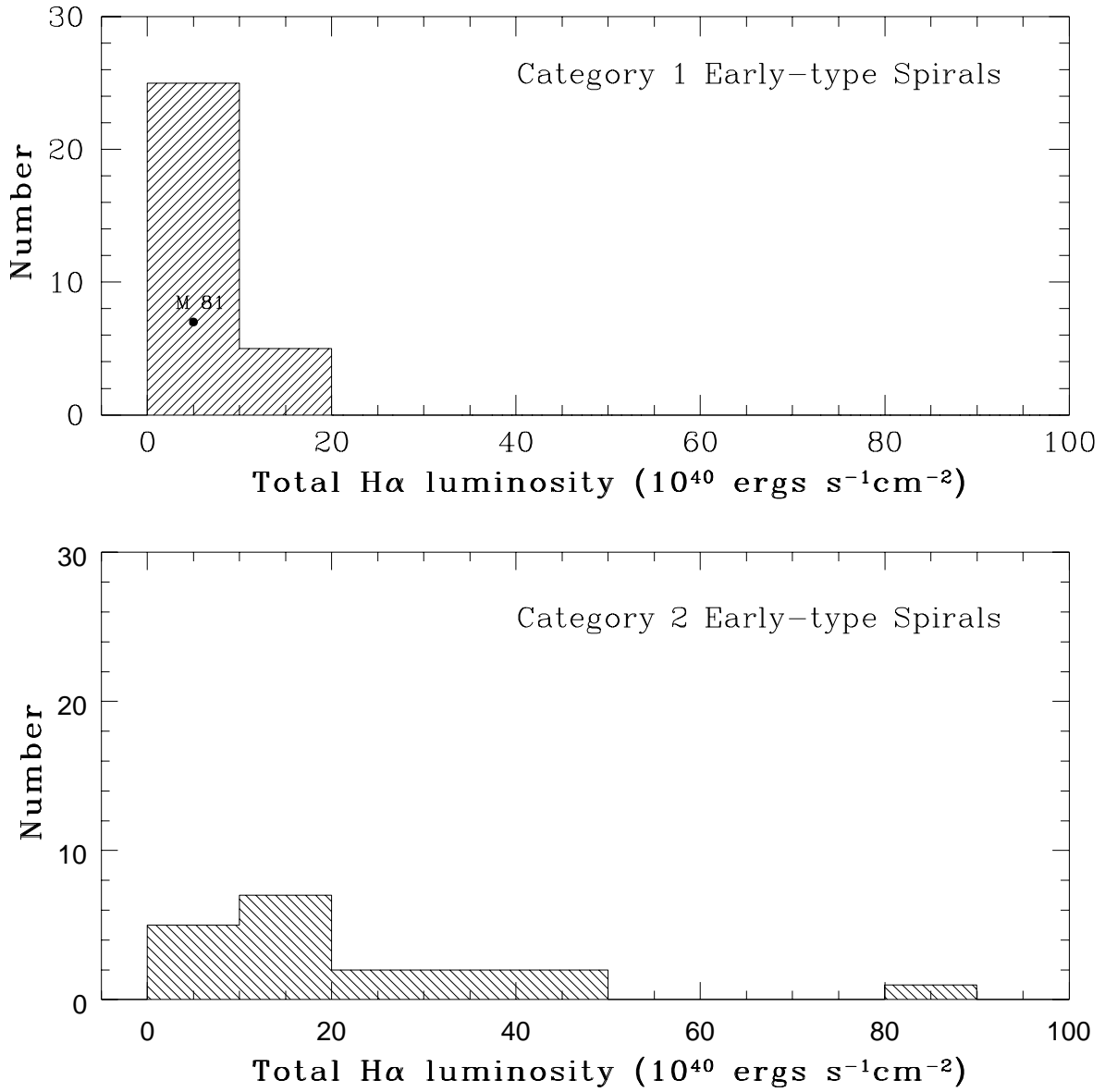


Fig. 4.— Histograms illustrating the distribution of total H α luminosity of Category 1 and Category 2 early-type spirals.

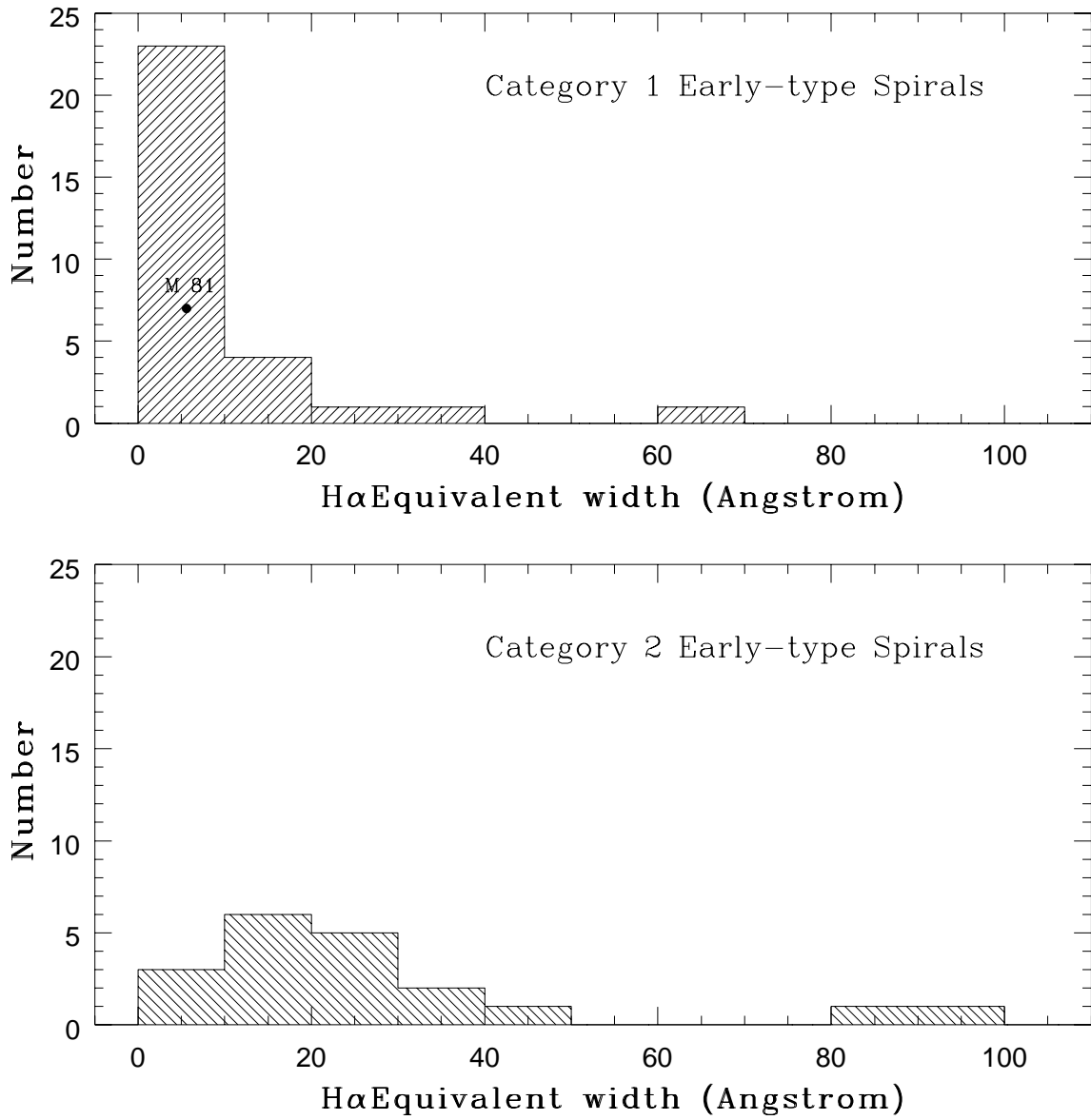


Fig. 5.— Histograms illustrating the distribution of H α equivalent widths of Category 1 and Category 2 early-type spirals.

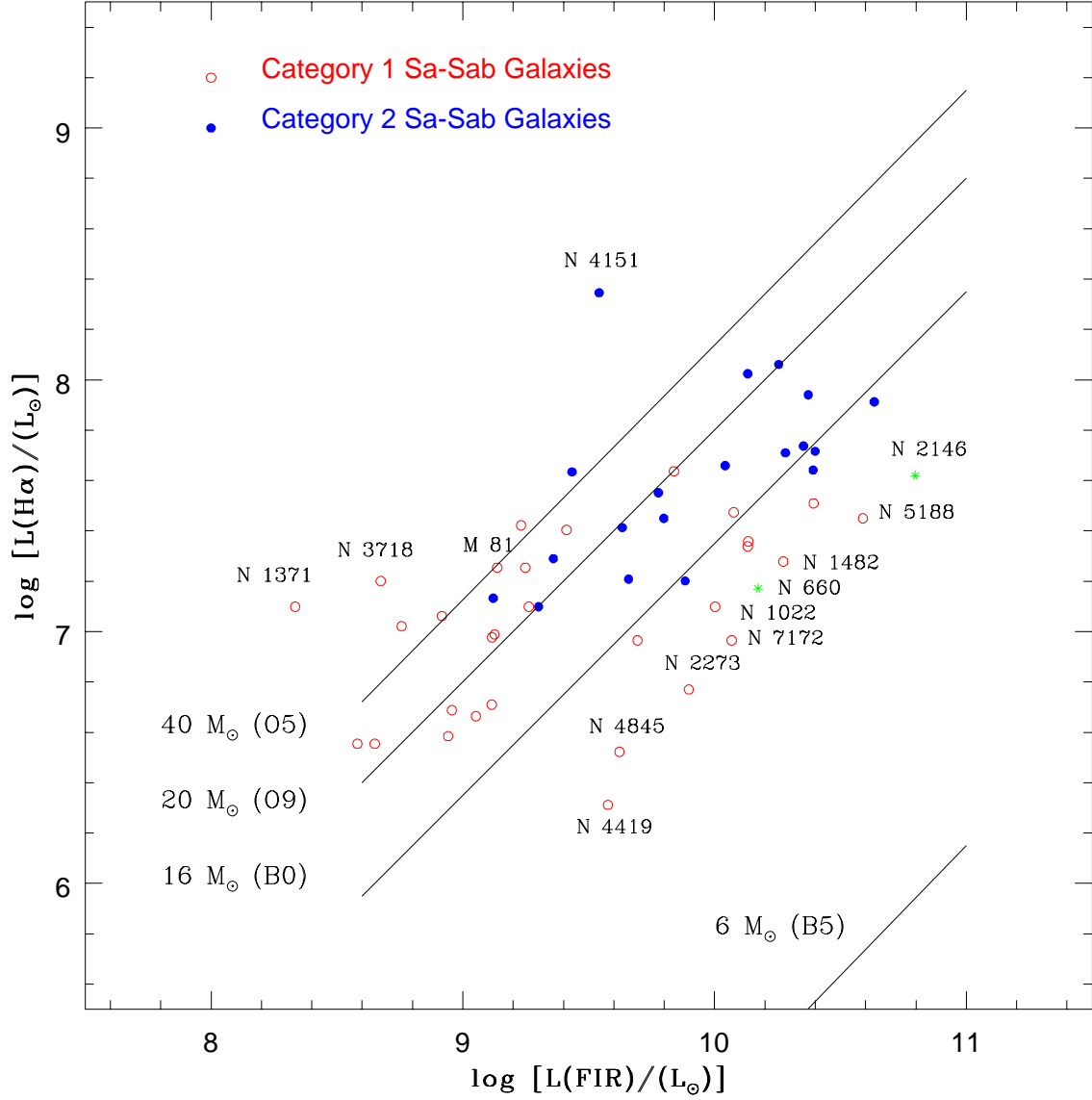


Fig. 6.— Correlation between the H α luminosity and the FIR (40-120 μ m) luminosity for 51 early-type spirals. The lines represent the $L(FIR/L(H\alpha))$ ratios expected for an H II region powered by stars of masses 40, 20, 16, and 6 M_\odot , respectively. The graph shows that O and B stars are capable of powering both the FIR and H α luminosities in these galaxies. Open circles represent Category 1 galaxies, and solid dots denote Category 2 galaxies. A star symbol is used to identify the two unclassified galaxies, NGC 660 and NGC 2146.

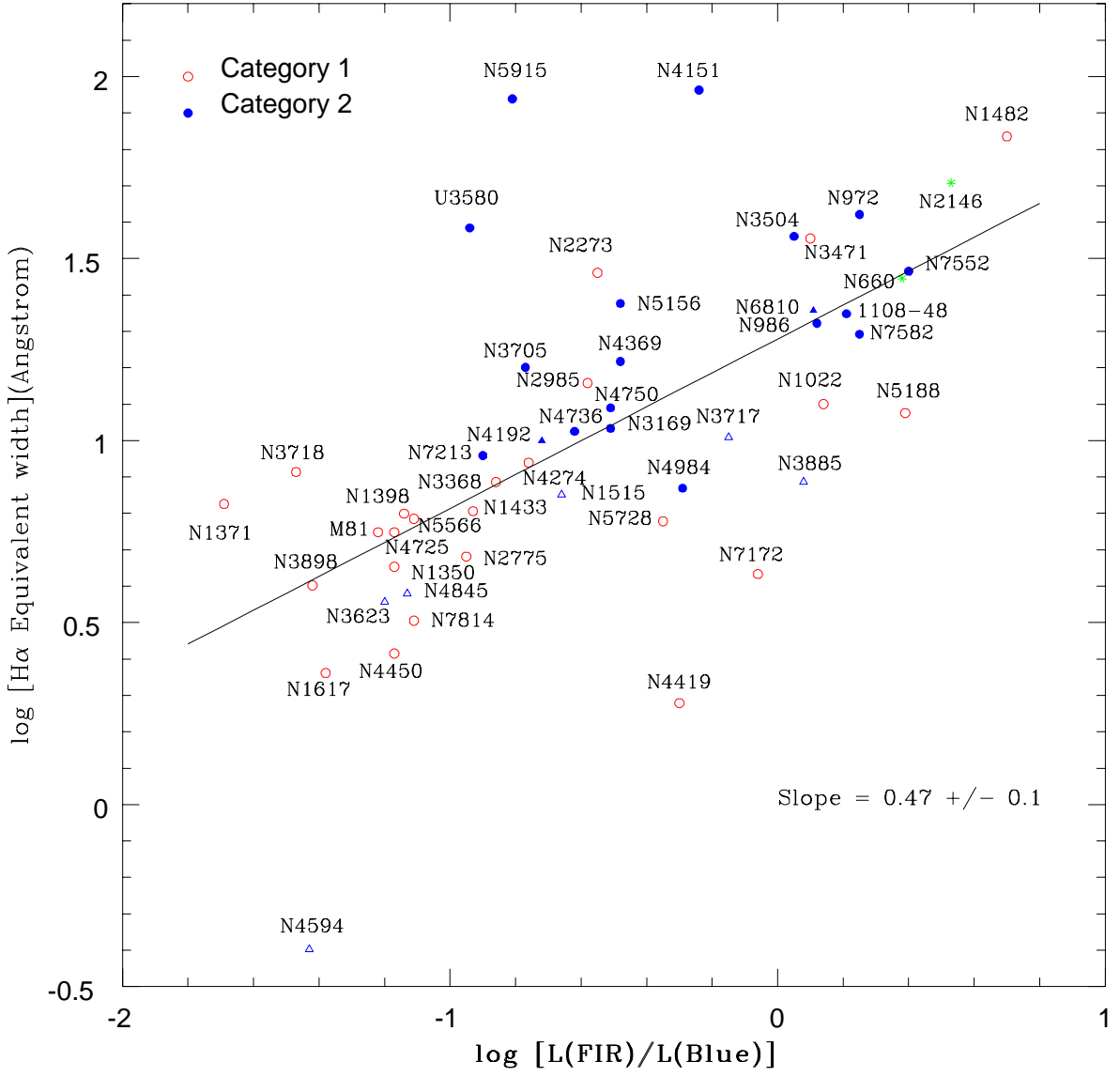


Fig. 7.— Correlation between the $\text{H}\alpha$ equivalent widths and the $\text{L(FIR)}/\text{L(Blue)}$ luminosity ratio for 51 early-type spirals. Open circles represent Category 1 galaxies and solid dots denote Category 2 galaxies. We have also identified highly inclined ($i > 75^\circ$) galaxies in each category as triangles and we do not find any strong dependence on inclination. A star symbol is used to identify the two unclassified galaxies, NGC 660 and NGC 2146 (NGC 660 also has $i > 75^\circ$). The least-squares fit for galaxies is shown as a solid line and all of the galaxies have been identified.

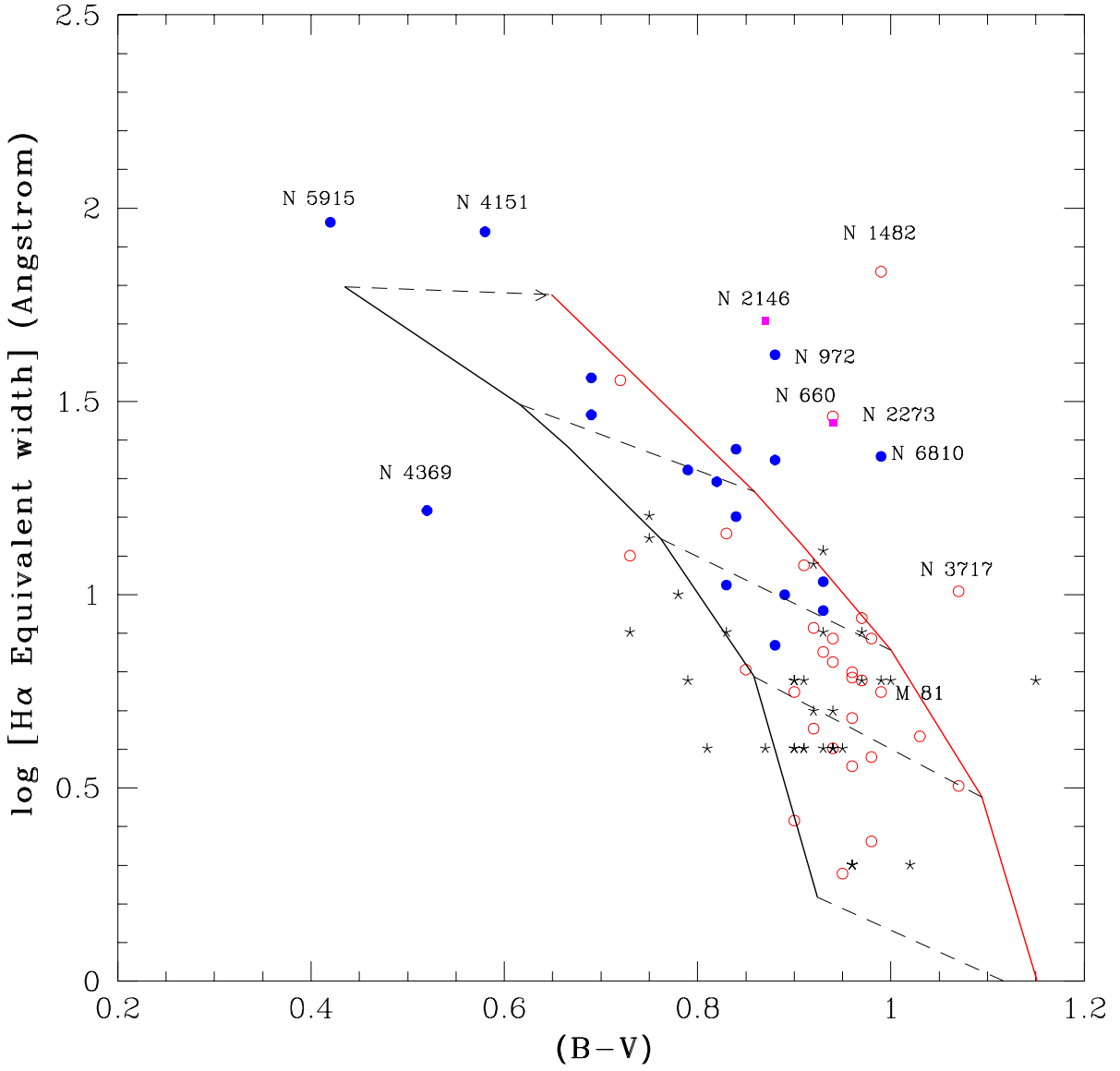


Fig. 8.— Correlation between the $(B-V)_e$ colors and $H\alpha$ equivalent widths for 49 early-type spirals. The symbols are the same as Figure 6. The red and black lines represent the loci of $(B-V)_e$ colors and $H\alpha$ equivalent widths for 15 Gyr old model galaxies that have evolved at different rates, with and without reddening respectively. The dashed lines indicate the direction of the reddening vectors for a constant star formation rate and exponentially decreasing star formation rates with with exponential timescales of 10, 5, 3.5 and 2.5 Gyrs. Kennicutt & Kent (1983) galaxies are plotted for comparison as five-pointed stars.

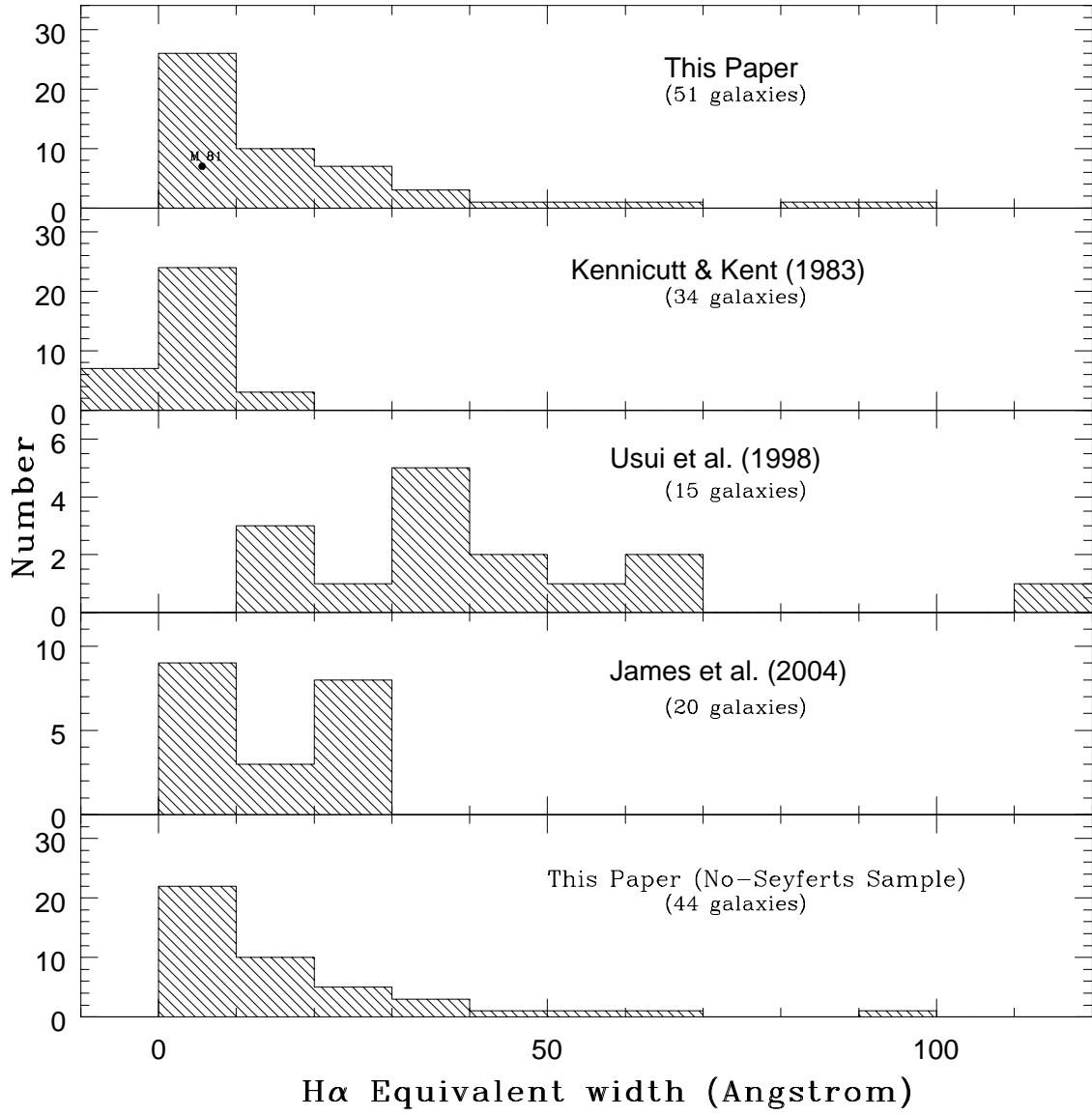


Fig. 9.— Comparison of H α equivalent widths of all 51 early-type spiral from our survey with the H α equivalent widths of Kennicutt & Kent (1983), Usui *et al.* (1998) and James *et al.* (2004). Bottom panel is our data after excluding Seyferts.

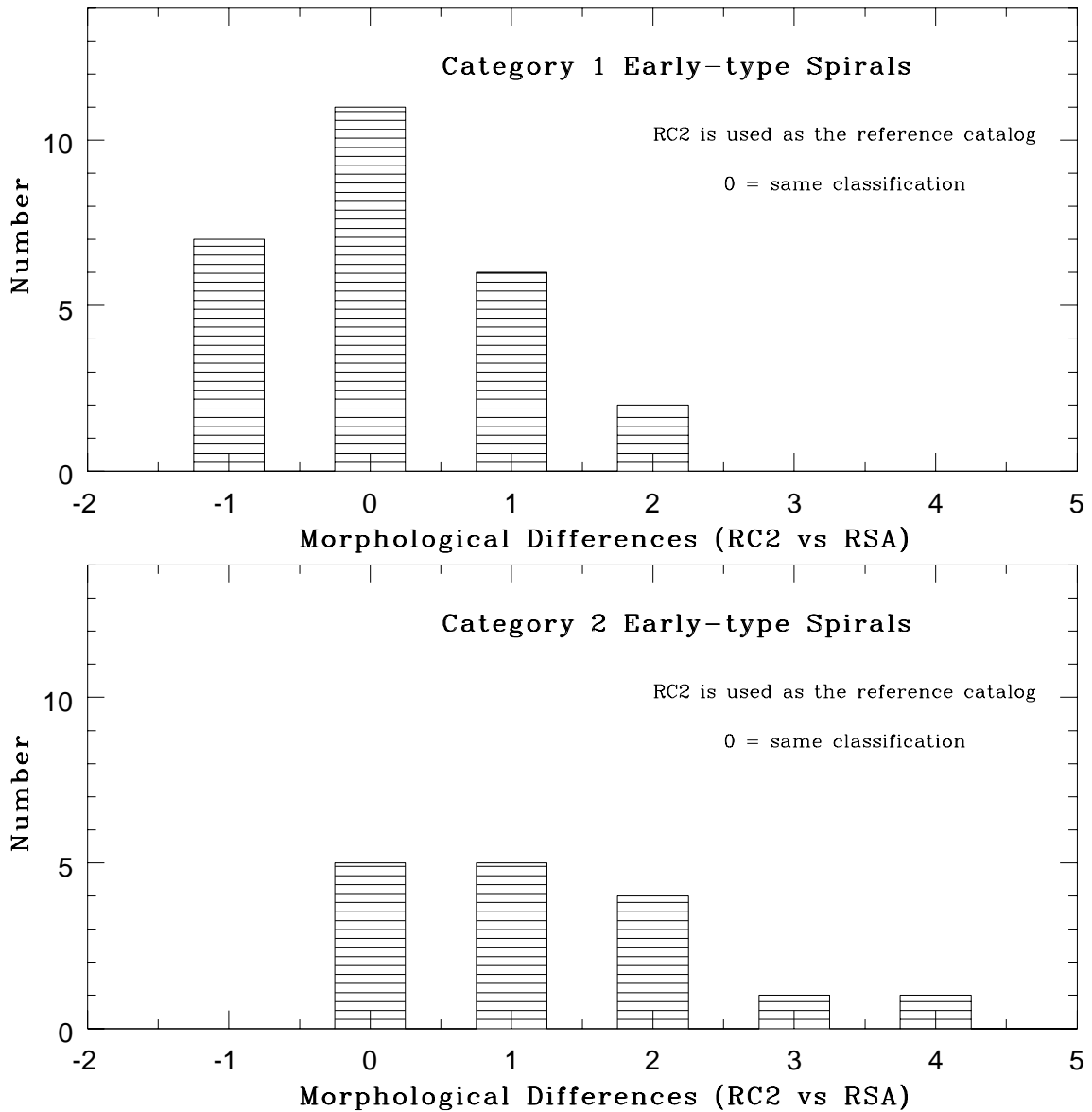


Fig. 10.— Comparison of morphologies from RSA and RC2 catalogs. The RC2 catalog is used as the reference catalog for Sa-Sab classifications. A “0” means that classifications match between RC2 and RSA. Differences in classifications for Category 1 galaxies are random. However, Category 2 galaxies are preferentially classified as later-types in the RSA catalog. See text for detail.

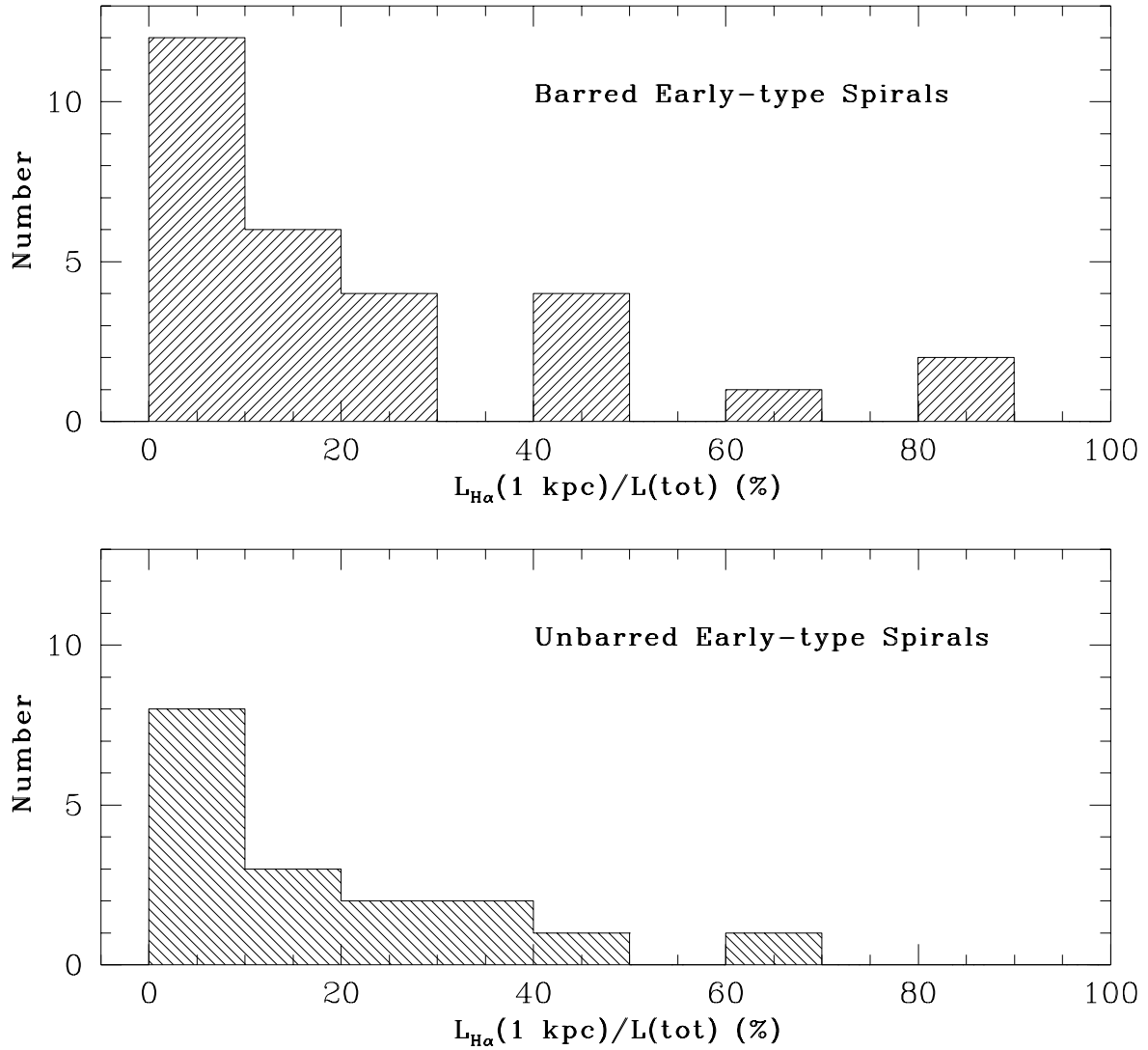


Fig. 11.— Histograms illustrating the ratio of H α emission from central 1 kpc to total H α luminosity for barred and unbarred galaxies.

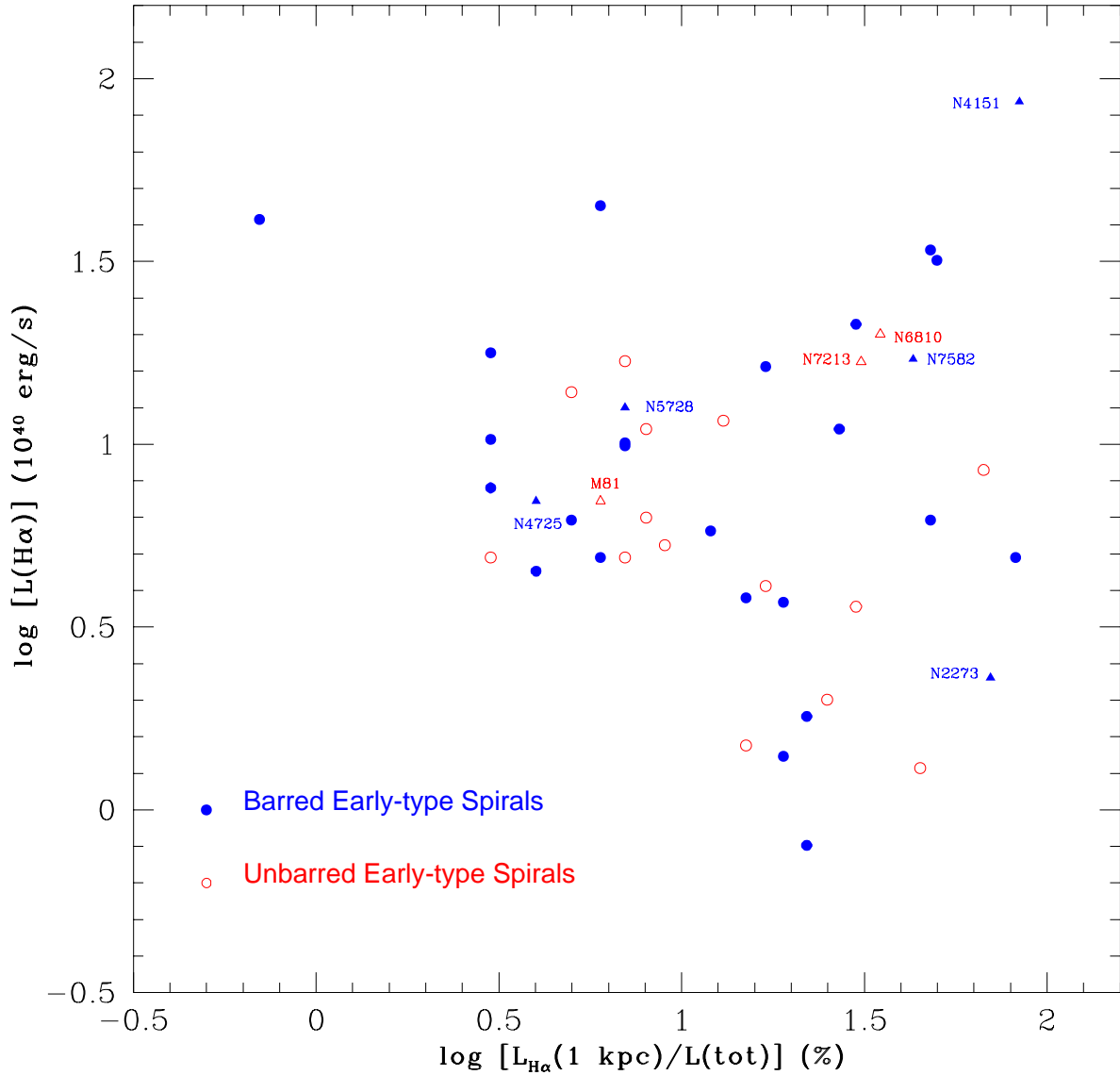


Fig. 12.— Correlation between the ratio of H α emission from central 1 kpc to total H α luminosity vs total H α luminosity for barred and unbarred early-type spirals.

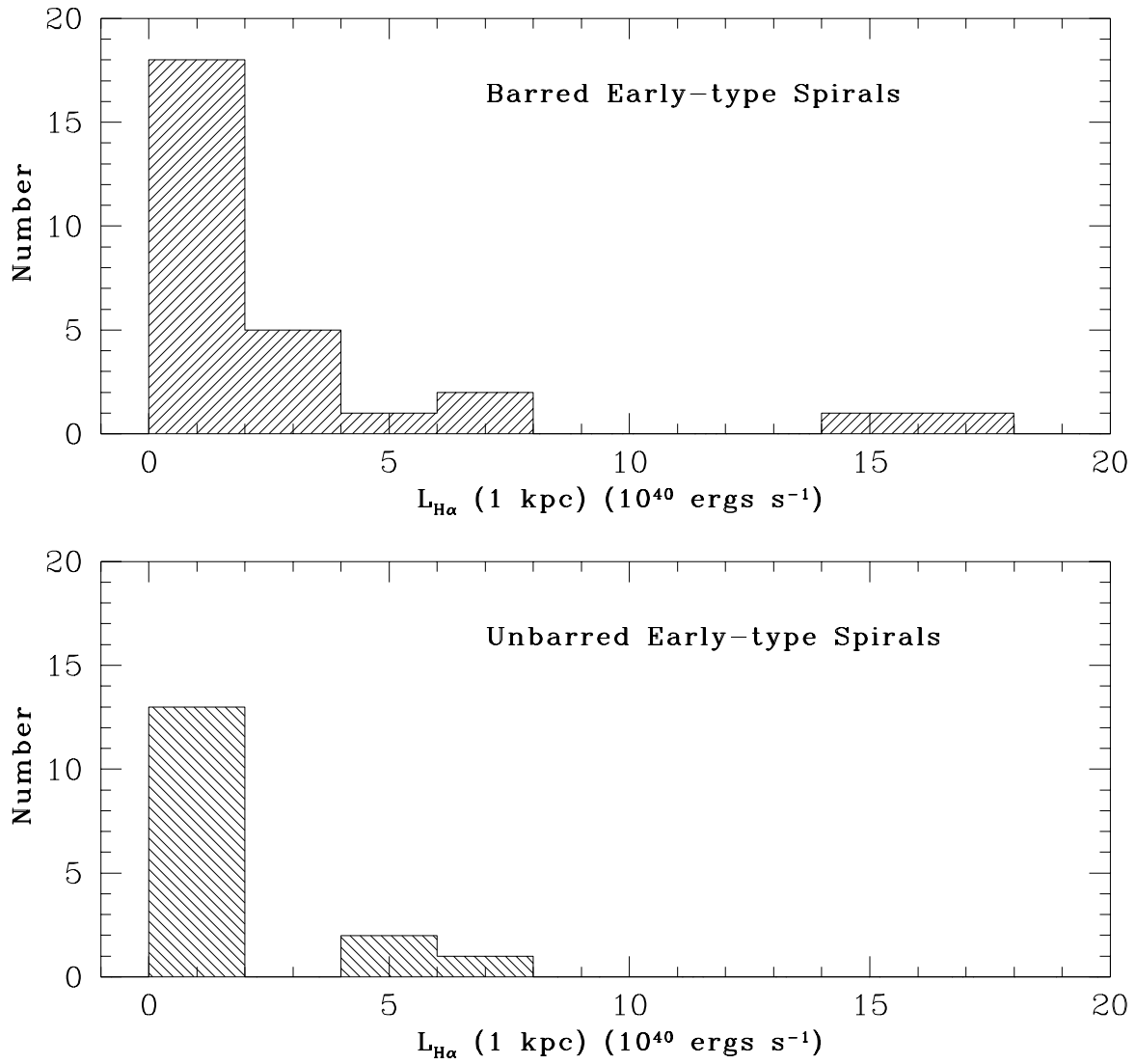


Fig. 13.— Histograms illustrating the H α luminosity from the central 1 kpc region for barred and unbarred galaxies.

Table 1. Galaxy Parameters^a

Galaxy	m(B) (mag)	size (arc min)	<i>i</i> (deg)	V _h (km s ⁻¹)	Distance (Mpc)
NGC 7814	11.26	5.9	68°	1047	15.1
NGC 660	11.37	7.2	77°	856	11.8
NGC 972	11.75	3.9	65°	1539	21.4
NGC 986	11.66	3.3	42°	1983	23.2
NGC 1022	12.13	2.5	28°	1503	18.5
NGC 1350	11.16	5.0	62°	1786	16.9
NGC 1371	11.43	6.8	53°	1472	17.1
NGC 1398	10.47	7.6	50°	1401	16.1
NGC 1433	10.64	5.9	27°	1071	11.6
NGC 1482	13.50	2.1	58°	1655	19.6
NGC 1515	11.17	5.7	89°	1169	13.4
NGC 1617	10.92	4.0	65°	1040	13.4
NGC 2146	11.00	5.3	36°	918	17.2
NGC 2273	11.63	3.4	50°	1844	28.4
UGC 3580	11.90	4.0	66°	1204	20.6
NGC 2775	11.09	4.6	39°	1135	17.0
NGC 2985	11.18	4.0	42°	1277	22.4
NGC 3031	7.59	22.1	60°	-43	3.6 ^b
NGC 3169	11.24	5.0	59°	1229	19.7
NGC 3368	10.05	6.7	50°	899	8.1
NGC 3471	12.98	1.9	64°	2076	33.0
NGC 3504	11.79	2.6	35°	1529	26.5
1108-48	13.64	2.4	53°	2717	35.2
NGC 3623	10.17	8.4	81°	806	7.3
NGC 3705	11.31	4.6	67°	1017	17.0
NGC 3717	11.87	6.1	90°	1731	24.6
NGC 3718	11.26	9.6	66°	987	17.0
NGC 3885	12.56	2.9	77°	1948	27.8
NGC 3898	11.71	4.7	46°	1172	21.9
NGC 4151	11.13	6.3	33°	989	20.3
NGC 4192	10.72	8.7	83°	-142	16.8
NGC 4274	11.12	6.5	72°	922	9.7
NGC 4369	11.80	2.4	0°	1052	21.6
NGC 4419	11.93	3.0	75°	-273	16.8
NGC 4450	10.90	5.0	50°	1958	16.8
NGC 4594	9.16	8.4	79°	1127	20.0
NGC 4725	9.91	10.5	43°	1207	12.4
NGC 4750	11.81	2.3	19°	1518	26.1
NGC 4736	8.85	12.2	33°	307	4.3
NGC 4845	12.07	4.8	81°	1228	15.6
NGC 4984	11.68	2.3	41°	1259	21.3
NGC 5156	11.92	2.4	24°	2983	39.5
NGC 5188	12.58	3.8	74°	2366	32.9
NGC 5566	11.29	5.6	71°	1518	26.4
NGC 5728	11.75	2.3	65°	2970	42.2

Table 1—Continued

Galaxy	m(B) (mag)	size (arc min)	<i>i</i> (deg)	V _h (km s ⁻¹)	Distance (Mpc)
NGC 5915	11.88	1.4	42°	2272	33.7
NGC 6810	11.40	3.2	82°	1995	25.3
NGC 7172	12.55	2.1	64°	2651	33.9
NGC 7213	11.35	2.1	...	1778	22.0
NGC 7552	11.31	3.5	31°	1609	19.5
NGC 7582	11.06	4.5	65°	1459	17.6

Table 2. Details of Observations

Galaxy	Epoch	Telescope	Hα filter	Exp. time	Standard ^a
NGC 7814	1999 Jan 13	KPNO 0.9m	6586/72	1200s	BD+28°4211
UGC 3580	1999 Jan 12	KPNO 0.9m	6586/72	1200s	BD+28°4211
NGC 2775	1999 Jan 13/Apr 10	KPNO 0.9m	6586/72	900s	BD+28°4211
NGC 2985	1998 Mar 25	APO 3.5m	6610/70	390s	PG0934+554
NGC 3368	1999 Jan 12	KPNO 0.9m	6586/72	1200s	BD+28°4211
NGC 3504	1999 Feb 13	APO 3.5m	6610/70	300s	Feige 34
NGC 3623	1999 Jan 12	KPNO 0.9m	6586/72	1200s	BD+28°4211
NGC 3718	1999 Apr 10	KPNO 0.9m	6586/72	1200s	Feige 34
NGC 3898	1999 Apr 12	KPNO 0.9m	6586/72	1200s	Feige 34
NGC 4151	1999 Apr 13	KPNO 0.9m	6586/72	1200s	Feige 34
NGC 4274	1999 Apr 9	KPNO 0.9m	6586/72	1200s	Feige 34
NGC 4369	1999 Feb 14	APO 3.5m	6610/70	300s	HZ 44
NGC 4594	1999 Apr 13	KPNO 0.9m	6586/72	1200s	Feige 34
NGC 4725	1999 Apr 10	KPNO 0.9m	6586/72	1200s	Feige 34
NGC 4750	1999 Feb 13	APO 3.5m	6610/70	300s	Feige 34
NGC 4736	1999 Apr 12	KPNO 0.9m	6586/72	1200s	Feige 34
NGC 4845	1999 Apr 13	KPNO 0.9m	6586/72	1200s	Feige 34
NGC 5566	1999 Apr 12	KPNO 0.9m	6586/72	1200s	Feige 34

^aM

Table 3. Summary of Results

Galaxy	$F_{(H\alpha+N[II])^a}$ ($10^{-12} ergs^{-1} cm^{-2}$)	Aperture (arcsec)	$L_{(H\alpha+N[II])}$ ($10^{40} ergs^{-1}$)	$EW_{(H\alpha+N[II])}$ (Å)	$L_{FIR(40-120\mu m)}$ ($10^{10} L_\odot$)	$L_{H\alpha}(1 \text{ kpc})$ ($10^{40} ergs^{-1}$)	$L_{H\alpha}(1 \text{ kpc})/L_{H\alpha}$ (%)	Reference ^b
Category 1 Early-type Spirals								
NGC 2985	2.8±0.5	116	16.9	14.4	0.69	1.1	7	1
NGC 5728	0.6±0.2	75.3	12.6	6.0	2.48	0.9	7	2
NGC 3717	1.6±0.2	180.6	11.6	10.2	1.19	1.5	13	2
NGC 5188	0.9±0.1	77.4	11.0	11.9	3.88	3.0	27	2
NGC 1398	3.3±1.2	215.0	10.3	6.3	0.17	0.3	3	2
NGC 5566	1.2±0.2	170	9.9	6.1	0.26	0.7	7	1
NGC 3471	0.7±0.1	20.4	8.9	35.9	1.36	5.1	57	2
NGC 3885	0.9±0.1	51.6	8.5	7.7	1.36	5.7	67	2
NGC 1482	1.6±0.2	48.9	7.4	68.5	1.87	3.7	50	2
NGC 4725	3.8±1.4	364	7.0	5.6	0.18	0.3	4	1
NGC 3031	45.3±13.5	...	7.0	5.6	0.14	0.4 ^b	6	3
NGC 3718	1.8±0.5	374.0	6.2	8.2	0.05	0.3	5	1
NGC 1022	1.2±0.2	77.4	4.9	12.6	1.00	4.0	82	2
NGC 1371	1.4±0.5	193.5	4.9	6.7	0.02	0.3	6	2
NGC 2775	1.4±0.8	170	4.9	4.8	0.18	0.1	3	1
NGC 1350	1.3±0.7	176.3	4.5	4.5	0.08	0.2	4	2
NGC 3898	0.7±0.4	204	4.1	4.0	0.06	0.7	17	1
NGC 3368	4.9±1.3	251	3.8	7.7	0.13	0.6	15	1
NGC 1433	2.3±0.8	197.8	3.7	6.4	0.13	0.7	19	2
NGC 4594	0.8±1.0	128 × 544	3.6	0.4	0.49	1.1	30	1
NGC 7172	0.3±0.1	53.8	3.6	4.3	1.17	0.7	19	2
NGC 2273	0.7±0.2	103.7	2.3	28.9	0.79	4.5	70	2
NGC 4450	0.6	127	2.0	2.6	0.13	0.5	25	4
NGC 4274	1.7±0.5	177	1.9	8.7	0.09	0.3	18	1
NGC 1515	0.9±0.2	307 × 172	1.8	7.1	0.11	0.4	22	2
NGC 7814	0.6±0.2	122	1.5	3.2	0.09	0.2	15	1
NGC 1617	0.6±0.6	111.8	1.4	2.3	0.04	0.2	14	2
NGC 3623	2.2±1.3	204	1.4	3.6	0.04	0.3	19	1
NGC 4845	0.5±0.2	88	1.3	3.8	0.42	0.6	45	1
NGC 4419	0.2	77	0.8	1.9	0.38	0.2	22	4

Table 3—Continued

Galaxy	$F_{(H\alpha+N[II])}^a$ ($10^{-12} ergs^{-1} cm^{-2}$)	Aperture (arcsec)	$L_{(H\alpha+N[II])}$ ($10^{40} ergs^{-1}$)	$EW_{(H\alpha+N[II])}$ (Å)	$L_{FIR(40-120\mu m)}$ ($10^{10} L_\odot$)	$L_{H\alpha}(1 \text{ kpc})$ ($10^{40} ergs^{-1}$)	$L_{H\alpha}(1 \text{ kpc})/L_{H\alpha}$ (%)	Reference ^b
Category 2 Early-type Spirals								
NGC 4151	17.5 ± 0.4	245	86.5	86.9	0.35	72.5	84	1
NGC 5915	3.3 ± 0.2	43.0	44.9	91.9	1.80	2.7	6	2
NGC 5156	2.2 ± 0.1	103.2	41.2	23.8	1.35	0.3	0.7	2
NGC 3504	4.0 ± 0.3	90	34.0	36.4	2.36	16.2	48	1
NGC 7552	7.0 ± 0.7	116.1	31.9	29.2	4.31	16.0	50	2
NGC 986	3.3 ± 0.4	114.0	21.3	21.0	2.25	6.3	30	2
NGC 972	3.7 ± 0.2	58.6	20.3	41.8	2.51	1.8	9	2
NGC 6810	2.6 ± 0.2	86.0	20.0	22.8	1.91	6.9	35	2
1108-48	1.2 ± 0.1	137.6	17.8	22.3	1.10	0.6	3	2
NGC 7582	4.6 ± 0.7	139.8	17.1	19.6	2.46	7.4	43	2
NGC 7213	2.9 ± 0.4	210.7	16.8	9.1	0.27	5.2	31	2
NGC 3169	3.0 ± 0.5	217.2	13.9	10.8	0.60	0.7	5	2
NGC 4750	1.4 ± 0.3	72	11.0	12.3	0.63	0.8	8	1
NGC 4192	3.0	380×380	10.1	10.0	0.43	0.7	7	4
NGC 3705	2.2	204	7.6	15.9	0.23	0.2	3	4
NGC 4369	1.1 ± 0.1	33	6.3	16.5	0.46	0.5	8	1
NGC 4984	1.1	80	6.2	7.4	0.76	2.9	48	4
UGC 3580	1.1 ± 0.1	136	5.3	38.4	0.13	0.5	9	1
NGC 4736	22.1 ± 4.2	476	4.9	10.6	0.20	0.3	7	1
Unclassified								
NGC 2146	4.6 ± 1.0	119.0	16.3	51.1	6.28	2.8	17	2
NGC 660 ^c	3.5 ± 0.3	173×585	5.8	27.9	1.49	0.7	12	1

^aFluxes have not been corrected for Galactic or internal extinction. $H\alpha + [NII]$ fluxes for galaxies observed by Koopman (1997) have 20-30% uncertainty.

^bNuclear $H\alpha$ luminosity for NGC 3031 is measured for central $800 \times 800 \text{ pc}^2$ region (Devereux, Jacoby & Ciardullo 1995)

^cNGC 660 was also included in Hameed & Devereux (1999). However, these are new large field of view $H\alpha$ observations that include the full extent of the galaxy.

References. — (1) This Paper; (2) Hameed & Devereux (1999); (3) Devereux, Jacoby & Ciardullo (1995); (4) Koopman (1997)

Table 4. Summary of Results II

Galaxy	Nuc. morph. ^a	Nuc. Sp. class ^b	Ref.	Bar ^c	Comments
Category 1 Early-type Spirals					
NGC 2985	PS ?	T1.9	2	N	
NGC 5566	ENER	L2	2	Y	Disturbed H α morphology.
NGC 5728	PS	S2	3	X	A tightly wound inner spiral arm and a loose outer spiral arm in the continuum.
NGC 3717	?	H	4	N	A prominent dust lane parallel to the major axis of the galaxy
NGC 5188	PS	H	4	Y	
NGC 1398	ENER	N	5	Y	A bar-ring morphology in H α .
NGC 3471	SB	H	6	?	
NGC 3885	SB	H	7	N	
NGC 3718	?	L1.9	2	Y	Disturbed continuum morphology.
NGC 1482	SB	?	A prominent dust lane parallel to the major axis of the galaxy. Filaments and/or chimneys of ionized gas extending perpendicular to the disk.
NGC 4725	ENER	S2	2	X	
NGC 3031	ENER/PS	S1	2	N	
NGC 1022	SB	H	8	Y	A tightly wound inner spiral arm and a loose outer spiral arm in the continuum.
NGC 1371	ENER	X	
NGC 2775	ENER	N	
NGC 1350	ENER	N	4	Y	A bar-ring morphology in H α . A tightly wound inner spiral arm and a loose outer spiral arm in the continuum.
NGC 3898	ENER	T2	2	N	
NGC 3368	ENER	L2	2	X	A bar-ring morphology in H α .
NGC 1433	ENER	N	4	Y	A bar-ring morphology in H α . A tightly wound inner spiral arm and a loose outer spiral arm in the continuum.
NGC 4594	?	L2	2	N	
NGC 7172	PS	S2	8	?	A prominent dust lane parallel to the major axis of the galaxy
NGC 2273	PS	S2	2	Y	
NGC 4450	ENER	L1.9	2	N	
NGC 4274	?	H	2	Y	
NGC 1515	ENER	X	
NGC 7814	?	N	
NGC 1617	ENER	?	
NGC 3623	ENER	L2	2	X	
NGC 4845	?	H	2	N	

Table 4—Continued

Galaxy	Nuc. morph. ^a	Nuc. Sp. class ^b	Ref.	Bar ^c	Comments
NGC 4419	?	T2	2	Y	
Category 2 Early-type Spirals					
NGC 4151	...	S1.5	2	X	
NGC 5915	Y	Asymmetric spiral arms in the continuum. $\text{H}\alpha$ morphology does not correspond with the major continuum features
NGC 5156	Y	
NGC 3504	...	H	2	X	
NGC 7552	...	H	4	Y	A dwarf galaxy at the end of the northern spiral arm
NGC 986	...	H	4	Y	A tidally disrupted dwarf galaxy at the end of the northern arm?
NGC 972	...	H	2	?	Dusty morphology. A possible bar-like structure crossing the nucleus
NGC 6810	...	S2	4	N	A prominent dust lane parallel to the major axis of the galaxy
1108-48	Y	A faint tidal tail leading to a star forming region 18 kpc north-east of the nuc.
NGC 7582	...	S2	9	Y	A prominent dust lane parallel to the major axis of the galaxy
NGC 7213	PS/ENER	S1	1	N	A giant $\text{H}\alpha$ filament is located approximately 17 kpc south of the galaxy with no counterpart in the continuum image.
NGC 3169	ENER	L2	2	N	
NGC 4750	...	L1.9	2	N	
NGC 4192	...	T2	2	X	
NGC 3705	...	T2	2	X	
NGC 4369	...	H	2	N	$\text{H}\alpha$ emission concentrated only near the nuclear region.
NGC 4984	X	
UGC 3580	N	
NGC 4736	...	L2	2	N	An anomalous $\text{H}\alpha$ tidal arm.
Unclassified					
NGC 2146	...	H	2	Y	Highly disturbed morphology with a prominent dust lane
NGC 660	...	T2/H	2	Y	Highly disturbed morph. Two prominent dust lanes perpendicular to each other

^a $\text{H}\alpha$ nuclear morphology: PS=Unresolved point source, ENER=Extended Nuclear Emission Line Region, SB=nuclear starburst. Nuclear regions of all category 2 and unclassified galaxies are resolved in $\text{H}\alpha$, but they do not meet the starburst or the ENER criteria as defined in the text. Hence their nuclear regions have not been classified morphologically.

^bClassification of the nuclear spectrum: S=Seyfert nucleus, H=HII nucleus, L=LINER, T=Transition objects, N=Seyfert-like, i.e. $\text{H}\alpha <$

$1.2 \times [NII]\lambda 6583$

^cBar classifications are taken from Tully (1988) : Y=Bar is present, N=Bar is absent, X=intermediate case, ?=No information.

References. — (1)Filippenko & Halpern (1984); (2)Ho, Filippenko, & Sargent (1997); (3)Phillips, Charles, and Baldwin (1983); (4)Veron-Cetty & Veron (1986); (5)Balzano (1983); (6)Lehnert & Heckman (1995); (7)Ashby, Houck, & Matthews (1995); (8)Sharples, Longore, and Hawarden (1984); (9)Unger *et al.* (1987)

Table 5. Morphological Classifications

Galaxy	NBG ^a	RC2 ^b	RSA ^c
Category 1 Early-type Spirals			
NGC 2985	Sab	Sab	Sab
NGC 5566	Sab	Sab	Sa
NGC 5728	Sa	Sa	Sb
NGC 3717	Sab	Sb	Sb
NGC 5188	Sa	Sb	Sbc
NGC 1398	Sab	Sab	Sab
NGC 3471	Sa	Sa	...
NGC 3885	Sa	S0/a	Sa
NGC 3718	Sa	Sa	Sa
NGC 1482	Sa	S0/a	...
NGC 4725	Sab	Sab	Sb
NGC 3031	Sab	Sab	Sb
NGC 1022	Sa	Sa	Sa
NGC 2775	Sab	Sab	Sa
NGC 1371	Sa	Sa	Sa
NGC 1350	Sab	Sab	Sa
NGC 3898	Sab	Sab	Sa
NGC 3368	Sab	Sab	Sab
NGC 1433	Sa	Sa	Sb
NGC 4594	Sa	Sa	Sa/Sb
NGC 7172	Sab	Sab	...
NGC 2273	Sa	S0/a	...
NGC 4450	Sab	Sab	Sab
NGC 4274	Sab	Sab	Sa
NGC 1515	Sa	Sbc	Sb
NGC 7814	Sab	Sab	Sab
NGC 1617	Sa	Sa	Sa
NGC 3623	Sa	Sa	Sa
NGC 4845	Sa	Sab	Sa
NGC 4419	Sa	Sa	Sab
Category 2 Early-type Spirals			
NGC 4151	Sab	Sab	Sab
NGC 5915	Sab	Sab	Sbc
NGC 5156	Sa	Sab	Sbc
NGC 3504	Sab	Sab	Sb
NGC 7552	Sab	Sab	Sbc
NGC 986	Sab	Sab	Sb
NGC 972	Sab	S0/a	Sb
NGC 6810	Sa	Sab	Sb
1108-48	Sab
NGC 7582	Sab	Sab	Sab

Table 5—Continued

Galaxy	NBG ^a	RC2 ^b	RSA ^c
NGC 7213	Sa	Sa	Sa
NGC 3169	Sa	Sa	Sb
NGC 4750	Sab	Sab	Sb
NGC 4192	Sab	Sab	Sb
NGC 3705	Sab	Sab	Sab
NGC 4369	Sa	Sa	Sc
NGC 4984	Sa	...	Sa
UGC 3580	Sa
NGC 4736	Sab	Sab	Sab

^a*Nearby Galaxies Catalog*, Tully (1988)

^b*Second Ref. Catalogue of Bright Galaxies*, de Vaucouleurs, de Vaucouleurs, & Corwin (1976)

^c*A Revised Shapley-Ames Catalog of Bright Galaxies*, Sandage & Tammann (1981)

This figure "f2a.jpg" is available in "jpg" format from:

<http://arxiv.org/ps/astro-ph/0506067v1>

This figure "f2b.jpg" is available in "jpg" format from:

<http://arxiv.org/ps/astro-ph/0506067v1>

This figure "f2c.jpg" is available in "jpg" format from:

<http://arxiv.org/ps/astro-ph/0506067v1>

This figure "f2d.jpg" is available in "jpg" format from:

<http://arxiv.org/ps/astro-ph/0506067v1>

This figure "f3a.jpg" is available in "jpg" format from:

<http://arxiv.org/ps/astro-ph/0506067v1>

This figure "f3b.jpg" is available in "jpg" format from:

<http://arxiv.org/ps/astro-ph/0506067v1>